Measurement driven, electron beam modeling and commissioning for a Monte Carlo treatment planning system with improved accuracy.

THÉBAUT Jonathan

Master of Science

Medical Physics Unit
Faculty of Graduate Studies and Research

McGill University

Montréal, Québec Canada

2009

A thesis submitted to the Faculty of Graduate Studies and Research of McGill University in partial fulfillment of the requirements of the degree of Master of Science in Medical Radiation Physics.

DEDICATION

I dedicate this thesis to the woman I love more than life itself, Miriam Viveros Thébaut. She brings a smile to my face, a tear to my eye and always inspired me, encouraged me and supported me during the course of this program. I love each moment we are together.

ACKNOWLEDGEMENTS

My sincere gratitude goes to my supervisor Dr. ***François DeBlois*** for his unconditional support, encouragement, wealth of brilliant ideas and invaluable guidance during the course of the project. He gave me freedom and trust in my work, great opportunities to introduce myself in the professional world of medical physics and many thanks for his continuous encouragements. My best gratefulness as well for reviewing my thesis by adding comments, suggestions, corrections and improvements. I would like as well to congratulate him for his recent position as a chef physicist at the Jewish General Hospital (JGH). I wish him all the best.

My sincere appreciation goes as well to Dr. ***Jan Seuntjens*** who played an enormous role. He was always there to discuss key point of the work and help us to realize our project. It would not have been possible without his help and expertise

My appreciation goes as well to Dr. ***Ervin Podgoršak*** as a true leader for maintaining the current world-renowned and excellent medical physics CAMPEP (Commission on Accreditation of Medical Physics Educational Programs) accredited program at McGill University (Montréal, Québec, Canada). I acknowledge him for providing me the opportunity to join this program and helping me to realize my dream.

I would like to express my gratefulness to the staff of medical physics Unit at the Montreal General Hospital (MGH) and at the Jewish General Hospital (JGH). In particular to ***Michael Evans*** for his help and expertise about electron beam measurements, to ***Krum Asiev***, Dr. ***Gabriella Stroian***, and ***Eric Reynard*** for theirs assistance and help to measure the data and for sharing times and knowledge with them during the commissioning of the linear accelerator at JGH. I also thank

Dr. ***Slobodan Devic*** for his assistance with the GafChromic® EBT films measurements. With this project I considerably improved my clinical experience thanks to a strong team like them. I also have to thank the technologs and dosimetrists for assistance with the accelerator and the use of Varian® ECLIPSE. I would like to express my gratitude to ***Andrew Alexander*** for the tremendous amount of time and patience he spent to help me understand the use of Monte Carlo, and computer-related problems. To Dr. ***Wamied Abdel-Rahman*** for assisting me in computer maintenance. I acknowledge the faculty members of the medical physics Unit program at McGill for their help, assistance and great teaching during the first eight months of the training program.

I would like to thank as well all the students that have gone through the medical physics program with me, for their kind help and assistance. In particular I thank ***Guillaume Landry***, ***Samy El-Jaby*** and ***David Rempel*** for being great friends and wish them all the best.

I would like to express a huge thankfulness to my family for their continuous love, encouragements and support. I thank my wife ***Thébaut Viveros Miriam***, my mother ***Gardien Régine***, my father ***Thébaut Patrick***, my brother ***Vatinel Victor*** and my sister ***Thébaut Constance*** for supporting me in doing what I like, for helping me financially. I shared with them the joys and frustrations I felt during the last two years, knowing this would not be possible without their strong support and love.

Finally I would like to acknowledge the *Lady Davis Institute* (LDI) for medical research financial assistance, the *Canadian Institutes of Health Research* (CIHR), the *Montreal Center For Experimental Therapeutics in Cancer* (MCETC), *« Les Fonds de la Recherche en Santé au Québec »*(FRSQ) and the Jewish General Hospital (JGH) for funding this work through the *Graduate training award in Experimental Therapeutics in Cancer.*

ABSTRACT

With the development of modern linear accelerators, the dosimetry of complex electron beams technique became a challenge for physicists. Over the past few years, lots of efforts have been done on developing accurate and fast dose algorithms for electrons. Numerous Monte Carlo (MC) models of therapeutic electron beams are presented in the literature. However, beam models built solely with manufacturer specifications of the medical accelerator do not systematically provide acceptable agreements with measurements. Clinically accurate beam models are crucial to MC treatment planning as electron dose calculations found in commercial treatment planning system (TPS) are generally inaccurate for complex geometry or with heterogeneities. Therefore, there is a strong motivation to use highly accurate MC simulations as standard information for commissioning commercial TPS. The current research project consists in developing an improved accurate electron beam model based on detailed information of the linear accelerator and to incorporate it into an in-house TPS: The McGill Monte Carlo Treatment Planning (MMCTP).

ABRÉGÉ

Avec le développement d'accélérateurs linéaires, la dosimétrie de techniques complexes de faisceaux d'électrons devient un défi pour les physiciens. Ces dernières années, des efforts considérables ont été faits pour développer un algorithme de calcul de dose précis et rapide pour les faisceaux d'électrons. De nombreux modèles Monte Carlo (MC) pour des faisceaux thérapeutiques d'électrons sont connus dans la littérature. Néanmoins, des modèles de faisceaux construits seulement avec les spécifications des constructeurs d'accélérateurs linéaires ne fournissent pas systématiquement des résultats en concordance avec les mesures. Au niveau clinique, des modèles de faisceaux précis sont d'une importance capitales pour les calculs de dose par Monte Carlo, dans la mesure où les algorithmes de calcul de faisceaux d'électrons présents dans les systèmes de plannification de traitements (SPT) commerciaux sont générallement imprécis dans des cas comportant des geométries complexes ou des hétérogénéités. Par conséquent, il y a une grande motivation à utiliser des simulations de Monte Carlo précis, comme information standard pour la mise en service des SPT commerciaux. La recherche présentée dans ce manuscrit vise à développer un modèle amélioré et précis de faisceaux d'électrons basé sur des informations détaillées d'accélérateurs linéaires et à incorporer ce modèle dans un SPT: le « McGill Monte Carlo Treatment Planning (MMCTP) ».

TABLE OF CONTENTS

LIST OF TABLES

LIST OF FIGURES

Chapitre 1
INTRODUCTION

Contents

1.1 Use of radiation therapy for cancer treatment and its goal.

According to the National Cancer Institute of Canada (NCIC), approximately 171,000 new cases of cancers will be diagnosed and 75,300 deaths as a result of cancer will occur in Canada just for the year 2009. This represents an increase of 4,600 newly diagnosed cases and 1,500 deaths compared to 2008. Cancer remains the second leading cause of mortality in Canada. In the past few years, significant advances have been made in the research of cancer treatment, and nowadays typical treatments modalities include radiation therapy (RT), chemotherapy, surgery, brachytherapy, targeted therapy, immunotherapy, and hormonal therapy. Half of the diagnosed patients will receive RT as the primary treatment procedure, or in conjunction with others techniques such as chemotherapy and/or surgery. The main goal of RT is to improve the quality of life of patients by the complete destruction or the shrinking of a tumor through the use of ionization radiation. Ionizing radiation can either be delivered from outside the body by an external source; this is called external beam therapy (EBT) or by radiation sources inserted inside the patient where higher total dose can be given to a smaller treated volume and in a shorter time: this is called internal radiation therapy or brachytherapy. Many forms of ionizing radiation are

used to treat different diseases: x-ray photons, protons, beta particles, heavy ions. However, the use of x-rays remains the most widely used method to treat cancerous tumors. Other particles are used more for their physical characteristics rather than their biological effects, which is the case for electrons. Electron beam therapy, subject that will be explained in greater details during the development of the thesis, is a unique therapeutic tool that offers advantageous treatments for certain types of tumors. The sites that are preferably treated with electrons are skin and lips, head and neck, upper-respiratory and digestive tract, total skin and boosts for breast cancers. Electrons offer an advantage in terms of physical characteristics such as dose uniformity over the tumor and healthy tissue sparing at depth. Over the past few years, interest has been shown to accurately calculate dose distributions in specific patient geometries from therapeutic electron beams. This is the goal of electron treatment planning systems.

1.2 Electron beam treatment planning systems.

A treatment planning system (TPS) consists in a computer and associated software that is used to generate dose distributions for specific beams and patient geometries. In the past, analytical methods and tables were used to fulfill that task. Nevertheless, for any method, the main goal is to determine the best treatment plan that will maximize the dose to the tumor while minimizing the dose to the healthy tissue. The important aspects of TPSs calculations algorithm are accuracy, precision, and calculation time.

Over the past few year, great works have been done on developing accurate and fast electron beam algorithms to model the electron transport thought matter. Such code is rated on his ability to handle heterogeneities (such as bones, air cavity), surface irregularities and real treatment situations. Due to the complexity of the physics of the electron transport and the lack of precise knowledge of the linear

accelerator head geometry, current electron beam models do not all provide good agreements with measured dose distributions under all possible clinical conditions. Electron treatments are often delivered clinically without previously calculating dose distributions because of a lack of accurate commercial electron dose calculation algorithms. The most widely used commercial dose calculation algorithm on the market is the Hogstrom [1] pencil beam algorithm. However, this algorithm does not properly model the electron transport in inhomogeneous phantoms and large dose discrepancies in the order of 10% and more are observed between calculated and measured dose [2–4]. Another method has been demonstrated to be very accurate under most geometries: the Monte Carlo (MC) algorithms that simulates electrons transport to calculate the dose. It is widely accepted that the use of MC transport in radiation therapy is one of the most accurate methods [5–8]. It has been shown that MC can handle multiple electron scattering in heterogeneity much more accurately than any other dose calculations algorithm. For instance, several groups have compared side by side Monte Carlo techniques and pencil beam algorithms and typically 3 to 9% differences in the mean dose within the planning target volume (PTV) has been observed in heterogeneity conditions [9, 10]. Therefore, MC algorithm is recognized as the gold standard to validate dose calculation algorithms. One main drawback of MC methods at this time is the long computing time necessary to obtain good statistics on the calculated values to compare with experimental measurements. Nevertheless, with the rapid increase of computing power, the availability of faster processors, the decrease of cost and the use of parallel processing, there is now a strong motivation to develop Monte Carlo electron base beam treatment planning systems.

1.3 Electron beam production.

During the first 50 years of radiotherapy that followed the discovery of x-rays by Roentgen in 1895, most dose deliveries were carried out with low voltage x-ray

generated machine. The invention of the Cobalt-60 unit by Dr. Harold Johns [11] in Canada in the early 1950s resulted in the use of higher-energy photon machines. Since then, the development of more modern machines has continued. Co-60 machines were gradually replaced by modern microwave-powered electron linear accelerators in the early 1970s. Commonly know as linacs, linear accelerators provide low and high energy x-ray, and generate a wide range of electron beam energies. Their design is compact and efficient. In the early 1980s over half of all megavoltage beam treatment units were linacs. At the present time, linacs are the most used treatment machines in radiotherapy. A medical linear accelerator installation is shown in Figure 1–1 page 4.

FIGURE 1–1 – *A medical linear accelerator [Varian Medical Systems] [12].*

The production of a high-energy medical beam starts in a linear accelerator by the acceleration of electrons through the use of non-conservative microwave radiofrequency (RF) fields generated by the use of special evacuated devices. The accelerator

structure receives the high power RF delivered by microwave generator such as magnetron or klystron, which catches the electrons and accelerate them to a velocity close the velocity of light. The RF ranges from 10^3 MHz (L band) to 10^4 MHz (X band) with the most common at 2856 MHz in the S band (2 - 4 GHz). The traveling wave accelerator (or waveguide accelerator) consists of a series of cylindrical accelerating cavities of length from 2.5 cm to 5 cm corresponding to the half wavelengths of the input microwave. Irises separate the cavities with circular holes in the center. Electrons are injected at one end of the waveguide by an electron gun and then accelerated in a straight manner in the evacuated accelerating waveguide. The linear accelerator is kept in vacuum to prevent electrical arcing between the disks and to avoid particles scatter.

Once the electrons have reached the end of the accelerating phase, they leave the standing wave accelerator and they are directed toward the beam transport system. However, linacs mounted isocentrically and designed with straight-through beam producing low energy beams (4 to 6 MeV), do not required beam transport between the accelerating waveguide and the target. Whereas high energy linacs (above 6 MeV) require a beam transport or beam bending magnet system to bend the electron toward the isocenter. For example, for Varian Clinac (Varian Inc. Palo Alto, CA) series used in this work, the electrons are directed toward a 270 degree achromatic bending magnet. This system has the advantage of offering achromatic properties that correct for energy spread and angular displacement.

For photon treatments, a target is inserted into the beam path and x-rays are produced in the forward direction through the slowing down of electrons (bremsstrahlung). However, if electrons are used instead, the target is retracted. The electron beam then continues through the vacuum before leaving the accelerating structure by the exit window. The electron beam continues its journey and enters the treatment head, which consists of various elements surrounded by high-density materials (lead,

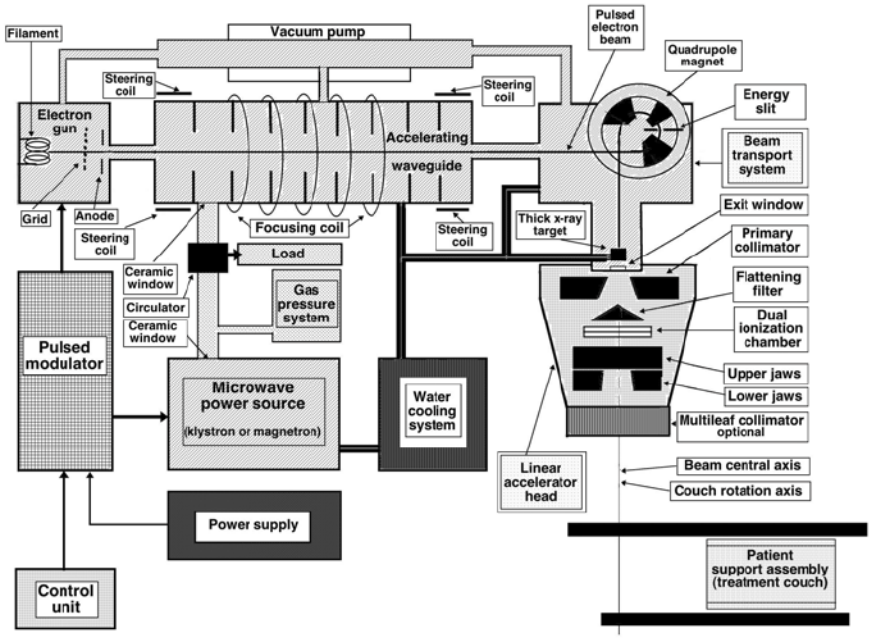

FIGURE 1–2 – *Diagram of a typical medical linear accelerator [13],*

tungsten), used for shielding purpose. The first component of the treatment head is a fixed primary collimator that collimates the beam in order to set the maximum field size. The electrons then strike a scattering foil to spread to a 3 mm diameter narrow pencil beam and to establish a uniform electron fluence. The thickness of the foil is such that the bremsstrahlung contribution to the electron beam is minimized as much as possible. In the case of x-ray photons, a carrousel rotates and replaces the foil by a flattening filter. This filter is used to make the beam intensity uniform across the treatment field (usually at a depth of 10 cm in a water phantom). The beam in the linac head is then incident on a dose monitoring chamber (system used to calibrate the output of the linac) made of several ion chambers. The beam is further collimated by movable collimator jaws. The major components of a medical linac are illustrated in Figure 1–2 page 6.

In electron mode of the linac, the beam needs further collimation. Since electrons are easily scattered by air molecules, the beam widths expands rapidly during

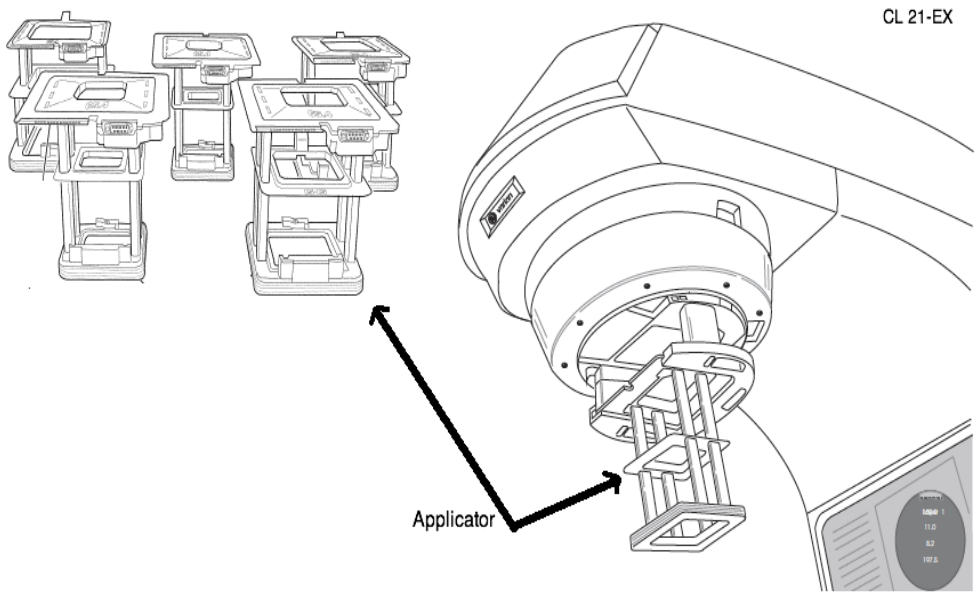

FIGURE 1–3 – *Illustration of the electron applicator mounted on a Varian Clinac 21-EX [12].*

the passage of electron through air. Hence, the beam must be collimated closed to the skin's patient. This is achieved by the use of applicators specially designed for electron therapy. The Varian Clinac 21-EX comes with a set of electron applicators of various sizes: (6×6) cm^2, (10×10) cm^2, (15×15) cm^2, (20×20) cm^2, and (25×25) cm^2 (see Figure 1–3 page 7). To further collimate and shape the beam to the tumor, metal plates (or electron cutouts) of different sizes and shapes are inserted at the bottom of the applicator. The medical linear accelerator used for this project is a state of art Varian Clinac 21EX that provides electron energies of 4, 6, 9, 12, 16 and 20 MeV and as well dual photon beam energies (6 MV and 18 MV). The linac is an isocentric machine with a source to axis distance (SAD) of 100 cm. It can supply a dose rate from 100 cGy/min to 600 cGy/min at depth of maximum dose (Z_{max}) for a (10×10) cm^2 and a source to axis distance (SSD) of 100 cm.

1.4 Proposed work.

The current research project consists of developing an improved accurate electron beam model using Monte Carlo (MC) techniques based on detailed information of the linac treatment head. To do so, a model for the dual scattering-foil Varian 21EX linac will be built for all available clinical electron energies for open beams, square, rectangular, circular and custom cutout shaped-beams. MC user codes BEAMnrc [14, 15] and DOSXYZnrc [16] will be used for the simulation. The verification of our model includes measurements of percentage depth dose curves and transverse dose profiles at various depths of clinical interest. These measurements will be used to tune-up the model.

1.5 Structure and scope of the thesis.

Chapter 2 gives an introduction on the interaction processes of photon and electron in matter. ***Chapter 3*** is presenting the electron beam dosimetry background required to understand and interpret the dose distributions. First, a general description of an electron depth-dose curve is presented. Then the concept of range and electron beam characteristics are explained. Specifications and measurement principles of electron energy along the beam axis (PDD) and dose profile are then discussed in detail. ***Chapter 4*** is concerned with Monte Carlo (MC) technique and this application in the field of medical physics. We describe the use of MC simulations in radiotherapy treatment planning, with an emphasis on the Electron Gamma Shower (EGS) [17, 18] source code along with an overview of the user codes BEAMnrc [14, 15] and DOSXZnrc [16]. In ***Chapter 5***, we will discuss the dosimetry equipments, and materials as well as the simulation techniques and methods used during the course of our project. Results and discussions are presented in ***Chapter 6***. We finally end this manuscript in ***Chapter 7*** with concluding remarks and discussions on future work.

References

[1] K. R. Hogstrom, M. D. Mills, and P. R. Almond. Electron beam dose calculations. *Phys. Med. Biol*, 26 :445–459, 1940.

[2] E. Mah J. Antolak J. W. Scrimger and J. J. Battista. Experimental evaluation of a 2D and 3D electron pencil beam algorithm. *Phys. Med. Biol.*, 34 :1179–1194, 1989.

[3] J. Cygler J. J. Battista J. W Scrimger E. Mah and J. Antolak. Electron dose distributions in experimental phantoms ; a comparison with 2D pencil beam code. *Phs. Med. Biol.*, 32 :1073–1086, 1987.

[4] K. R. Shortt, C. K. Ross, A. F. Bielajew, and D. W. O Rogers. Electron beam dose distributions near standard inhomogeneities. *Phs. Med. Biol.*, 31 :235–249, 1986.

[5] Mackie T R. Application of the Monte Carlo method in radiation therapy. *The dosimetry of Ionization Radiation*, 3 :541 – 620, 1990.

[6] Mohan R and Antolak. Monte Carlo techniques should replace analytical methods for estimating dose distribution in radiotherapy treatment planning. *Med Phys*, 28 :123–126, 2001.

[7] Rogers D W and Bielajew A F. Monte Carlo techniques of electron and photon transport for radiation dosimetry. *The dosimetry of Ionization Radiation*, 3 :427–539, 1990.

[8] Rogers D W and Bielajew A F. The role of Monte Carlo simulation of electron transport in radiation dosimetry. *Int. J. Radiat. Appl. Instrum*, 42 :965–74, 1991.

[9] York E Wang L and Chui C S. Monte Carlo evaluation of 6 MV intensity modulated radiotherapy plans for head and neck and lung treatments. *Med. Phys.*, 29 :2705–2717, 2002.

[10] Pawlicki T and Ma C M. Monte Carlo simulation for MLC-based intensity-modulated radiotherapy. *Med. Dosim.*, 26 :157–168, 2001.

[11] Epp E.R. Johns H.E., Bates L.M. 1,000-curie cobalt 60 units for radiation therapy. *Nature*, 168 :1035–6, 1951.

[12] Varian Medical System Web-Page. http ://www.varian.com/.

[13] Ervin.B. Podgorsak. *Radiation Physics for Medical Physicists*, volume 1 edition. Springer Berlin Heidelberg New York., New York, 2005.

[14] Rogers D W O, Faddegon B A, Ding G X, Ma C M, Wei J, and Mackie T R. BEAM : A Monte Carlo code to simulate radiotherapy treatment units. *Med. Phys.*, 22 :503–524, 1995.

[15] Rogers DWO, Ma Ding, GX Walter, Sheikh-Bagheri and Zhang GC. BEAMnrc users manaual. Pirs 509a (rev f), NRCC - Canada Ottawa - National Research Council., 2001.

[16] Walters B, Kawrakow I, and Rogers D W O. DOSXYZnrc users manual. PIRS 794revB, NRCC, 2004.

[17] Kawrakov I and Rogers D W O. The EGSnrc code system : Monte Carlo simulation of electron and photon transport. Pirs-701, NRCC - Canada Ottawa - National Research Council., 2003.

[18] Kawrakov I and Rogers D W O. EGSnrc / BEAMnrc / DOSXYZnrc. EGS electron gamma source. Pirs, NRCC - Canada Ottawa - National Research Council., 2003.

Chapitre 2
PHYSICS OF PARTICLE INTERACTIONS

Contents

2.1 Ionization radiation.

Ionization is defined as the process by which a neutral atom or a molecule is converted into a ion by gaining or loosing a charged particle such as an electron. Depending on the ionizing particles involved, radiation can be classified into two categories; *directly ionizing radiation* and *indirectly ionizing radiation.*

Charged particles such as electrons, protons, and alpha particles, as they penetrate matter, deposit energy in the medium by direct Coulomb interactions with orbital electrons of atoms. The energy transferred to the medium along the track is absorbed in a large number of small increments. The energy involved may be used to excite the atom by moving an orbital electron to an unstable higher quantum shell; this process is termed as excitation. Alternatively, the energy carried by the charged particle may be high enough to overcome the electron binding energy in a shell, i.e. high enough to knock out an orbital electron and thus to ionize the atom. The ejected electron may be sufficiently energetic to produce on its own a secondary ionizing track, known as a delta (δ) ray. The process of direct energy deposition by charged particle resulting in ionization is known as *directly ionizing radiation.*

The other category of radiation is *indirectly ionizing radiation.* Uncharged particles, such as neutrons and photons, deposit energy in the medium through a release in the medium of charged particles that will later deposit energy when interacting with matter. Photons liberate electrons and positrons while neutrons release protons or heavier ions.

Radiobiologically, ionizing radiation transfers energy to the absorbing material in cells. The process, if energetic enough, transforms the cells by destructing them, or preventing their replication by damaging the molecules DNA (Deoxyribonucleic acid). The energy deposited per unit mass in the absorbing medium such as body tissues, is a concept known as absorbed dose. So dose deposition into a medium that may produce biological damage is only done directly by charged particles. Indirectly ionizing radiation is not directly responsible for biological damage. Only the resulting interactions that produce charged particles are responsible for energy deposition into the material. For the case of a photon passing into an absorbing tissue, electrons may be set motion and will travel through the tissue where ionization, excitation or even molecular bonds breakage may occur. The processes by which a photon may interact with matter to produce high-speed electrons are explained in the next section.

2.2 Interaction of uncharged radiation with matter.

In this section, we discuss the basic physics processes by which photons interact with matter. Depending on the photon energy or the medium properties, photons may either interact:

- with the absorber atom as a whole.
- with the nucleus of the absorber atom.
- or with an orbital electron of the absorber atom.

The probability of photon attenuation by the absorbing medium depends on the photon energy as well as the density and atomic number Z of the absorber and can be

classified into five major types of interaction. One of these is the interaction between the photons and the nucleus of an atom: the *photodisintegration* or *photonuclear* interaction. This process is only important at high photon energy, typically energy larger than 10 MeV. The other four dominant processes are *Coherent scattering (Rayleigh), photoelectric effect, incoherent scattering (Compton effect)*, and *pair production.*

Coherent scattering (*Rayleigh*) occurs when a photon interacts with a bound orbital electron, i.e. with the absorber atom as a whole. The scattered photon has essentially the same incident energy and it is emitted in a slightly different direction. Practically no energy is transferred to the medium and the outgoing photon is elastically scattered thought a very small angle. This effect is more probable in high atomic number Z material and at low photon energies. It is thus negligible for therapeutic situations, i.e. for mega-voltage photons interacting with low Z material such as tissue.

As the photon energy increases, *photoelectric effect* becomes more probable to occur as compared to coherent scattering process. The photoelectric effect discovered by Hertz in 1887 and explained by Einstein in 1905 is the interaction by which an incident photon of energy $h\nu$ interacts with an atom by ejecting a bound orbital electron from one of the orbital shells (K, L, M, N, ...). The ejected electron, called photoelectron, emerges with an energy of $h\nu$ - E_{B}, (E_{B} is the binding energy of the shell from which the electron is ejected). As a result of this process, a vacancy is created in the shell leaving the atom in an excited state. Then, different processes occur depending on the composition of the absorber. One of these is described by the emission of a characteristic [1] photon, which results when an electron from higher electronic shell fills the lower vacancy one. A competing effect to the emission of a

1. *The term characteristic is used because the photon is characteristic of the energy difference between the two shells.*

characteristic photon is the emission of an *Auger electron*: monoenergetic electron produced with the energy transferred from a vacancy shell. The photoelectric effect probability, or photoelectric mass attenuation coefficient, decreases approximately with the third power of photon energy as $\frac{1}{(h\nu)^3}$ at low photon energy which gradually transform into $\frac{1}{h\nu}$ at high energy. The photoelectric attenuation depends also strongly on the atomic number Z of the absorbing material. The cross section per electron depends upon Z^3 and $Z^{3.8}$ for high and low Z materials respectively.

As the energy of the incident photon increases it becomes less and less probable for photoelectric effects to happen, and *Compton scattering* takes over. Compton process is an incoherent effect that can be explained as follows: a photon interacts with a target and transfers energy to a free [2] or unbound electron. Unlike photoelectric effect the photon does not disappear, but it is deflected at a given scattering angle. The photon looses energy in the process by transferring part of its kinetic energy to the recoil loosely bound electron. One of the interesting aspects in the Compton process is that the photon energy, used to set in motion the electron, is independent on the atomic number Z of the absorbing material. So unlike photoelectric effect and Rayleigh scattering, Compton process is strictly a photon-electron interaction where incident photon and electron binding energy play a key role in the process. As an example, when a mega-voltage photon undergoes Compton scattering, a large fraction of the incident energy in transferred to the unbound electron, hence leaving the scattered photons with a small fraction of the incident photon's energy.

The last process, which has a photon energy threshold of 1.02 MeV, is the *pair production* process. If a photon interacts strongly with the electromagnetic field of

2. *The term « free electron » is not used appropriately since no electrons are really free. Indeed, outer shell electrons are bound to the atom by a few electron volts and therefore not free. However, the term « free electron » can be used if the corresponding electron binding energy is a small fraction of the incoming photon energy.*

an atomic nucleus and it may suddenly become a pair of positron (e+) and electron (e-). The positron transfers its energy by the same processes as an electron does, i.e. by ionization, excitation and bremsstrahlung (bremsstrahlung effect will be explained in the next section). After loosing all its kinetic energy and thus coming to rest, the positron combines with a free available electron in its neighborhood. This gives rise to an annihilation where the positron and the electron mass is converted to an energy release of 1.022 MeV. Generally for energy, charge and momentum to be conserved, two photons, each with energy of 0.511 MeV, are emitted practically in opposite direction. Since the pair production process occurs in the electromagnetic field of the nucleus, the probability increases rapidly with atomic number Z: the attenuation coefficient per atom varies with the square of the atomic number Z^2.

Instead of interacting with the atomic nucleus, the photon may interact with an orbital electron producing a positron-electron pair in the presence of the original orbital electron. Therefore three particles leave the interaction site. This effect is called *triplet production*.

As mentioned above, a photon will undergo one of the various interactions with a probability that depends on the photon's energy and on the atomic number Z of the attenuator. This is well illustrated in Figure 2–1 page 16, where the relative predominance of the three dominant processes responsible for energy deposition into the medium is shown (Rayleigh effect does not transfer energy). The curves correspond to an equal probability between two interactions processes. The left curve represents the points where the atomic coefficients for the photoelectric effect (τ) and Compton effect (σ) are equal, i.e. $\tau = \sigma$. Whereas the right curve represents the points where atomic coefficients for Compton effects (σ) and pair production (κ) are equal, i.e. $\sigma = \kappa$.

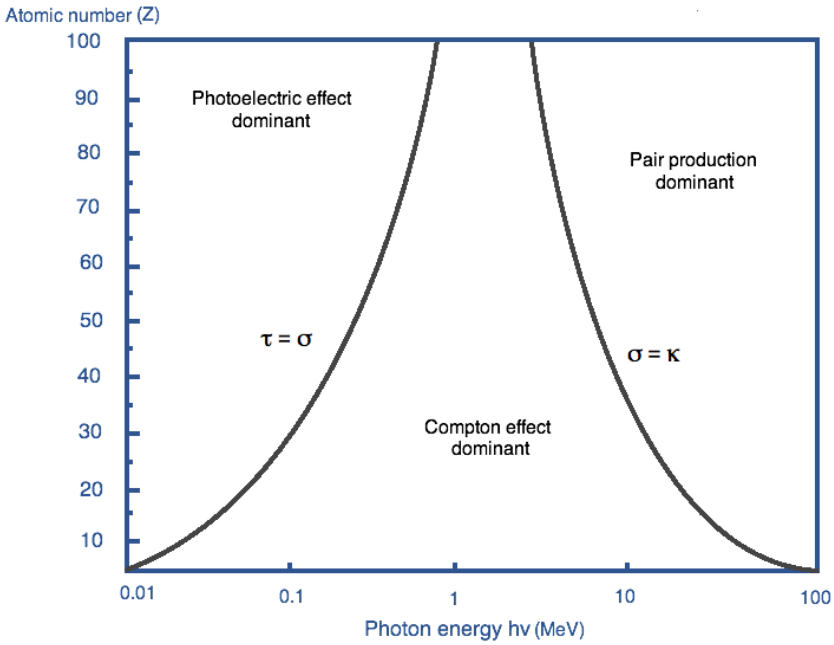

FIGURE 2–1 – *Regions of relative predominance of the three main processes of photon interactions with an absorber : photoelectric effect, Compton scattering, and pair production (Reproduced from Ervin.B. Podgorsak, Radiation Physics for medical Physicists, page 246) [1].*

2.3 Electron interactions with matter.

2.3.1 Types of electron Coulomb-force interactions.

The previous section explains how photons interact with matter. However, they can also go through a medium without interacting at all, i.e without exchanging energy with it. They can also lose their energy through various photon interactions (the photoelectric effect, the Compton effect, pair production, etc..., see Section 2.2 page 12). When a photon interacts with the surrounding medium, one or more electrons are set in motion and carry away part of the initial photon energy. These electrons deposit their energy directly into the medium. However, the process through which charged particles exchange energy with the medium is distinctly different from the photon's processes. Indeed, during its journey an electron suffers multiple collisions with the atomic nuclei and the orbital electrons. Most of theses interactions

transfer only a small fraction of the energy of the moving charged particle. A therapeutic electron beam loses approximately [3] 2 MeV of kinetic energy per cm of water. A 1 MeV electron will undergo about 10,000 interactions in water before coming to rest. This mutual energy exchange is achieved through Coulomb interactions between the travelling electron and the electric fields of the atoms of the medium. The penetration of an electron through water-like tissue depends on its energy and the perpendicular distance by which the electron misses making a direct hit with the atomic nucleus (or impact parameter b). Typically two different energy losses may occur:

- collisional losses through soft and hard collisions.
- radiative collisions.

The mechanism for *collisional looses* involves the ionization and the excitation of an atom. The probability for a given process depends on the atomic number of the medium, on the electron energy and the distance of interaction. If the impact parameter b of the electron is very large compared to the atomic radius, then the electron will undergo a *soft collision* with the whole atom. During the collision a small amount of energy, in the order of few electron volts, is transferred to the atom. The atom becomes excited and an electron from an inner quantum shell may jump to an outer shell. The result is the emission of visible photons if the interacting medium is a gas, and in heat dissipation for solid material. Under certain conditions coherent bluish-white light, called *Čerenkov* radiation, is emitted by the absorbing medium. This phenomenon occurs when the electron velocity exceeds the speed of light in the medium.

When the electron is very close to the atom, i.e. when the interaction occurs within the atomic dimension, it becomes more likely that the electron transfers its

3. *Averaged over the distance traveled by the electron i.e. from the first interaction to the point where it comes to rest.*

energy to a single electron. This is defined as a *hard collision* (or « knock-on collision »). The electron can therefore lose a large fraction of its kinetic energy. If enough energy is transferred to overcome the electron binding energy, the electrons can be removed from their shell and the atom become ionized. The ejected electron is called a delta (δ) ray (or secondary electron) and might be responsible on its own for further ionizations and excitations. The δ-ray dissipates its energy along a separate track, (usually referred as a « spur »), and therefore might experiences the same processes and fate as the primary electron. Soft collisions involve Coulomb's interactions with « distant » atoms, and are thus clearly more probable than near hit collisions. They roughly account for half of the energy exchanged with the surrounding medium.

Finally if the impact parameter b is much smaller than the atomic radius, another type of interaction may occur within the Coulomb field of the nucleus. Indeed, due to its relative small mass, the electron may also interact with the electromagnetic field of the atom's nucleus. The energy lost by the travelling electron could be large enough that the electron would suddenly decelerate, and be deflected from its original path. During that process, some of its energy is transferred as electromagnetic radiation knows as *bremsstrahlung* [4] . This is the fundamental process for the production of x-rays in a linac of x-ray machine. This type of collision between an electron and a nucleus is referred to as a *radiative collision.*

2.3.2 Collisional and radiative stopping power.

In the preceding section it has been shown that when an electron travels trough a medium, it subsequently transfers its energy to the medium by a multitude of relative small interactions with the electrons and atoms of the medium. The rate at which

4. *has its origin from German for « braking radiation »*

electron energy is lost along its track is a well-defined quantity knows as the stopping power. The linear stopping power is defined as the expectation value of the rate at which an electron losses its energy per unit of length travelled, with units of $\frac{\text{MeV}}{\text{cm}}$. Generally a more useful quantity is obtained by dividing the linear stopping power by the density, and this gives the mass stopping power expressed as:

$$\left(\frac{S}{\rho}\right)_{\text{tot}} = \frac{1}{\rho}\frac{\overline{dE}}{dx} \qquad \left[\text{MeV}\cdot\text{cm}^2/\text{g}\right] \tag{2.1}$$

Commonly, the total mass stopping power S_{tot} is given as the sum of the radiative stopping power S_{rad} and the collisional stopping power S_{col} (Equation 2.2 page 19).

$$\left(\frac{S}{\rho}\right)_{\text{tot}} = \left(\frac{S}{\rho}\right)_{\text{col}} + \left(\frac{S}{\rho}\right)_{\text{rad}} \qquad \left[\text{MeV}\cdot\text{cm}^2/\text{g}\right] \tag{2.2}$$

The collisional (ionization) stopping power is the rate of energy loss resulting from the sum of soft and hard collisions. However, the radiative stopping power is the result of interactions of the travelling charged particles with the nuclei of the absorber (bremsstrahlung production alone). Only light charged particles such as electrons loose appreciable energy through this process. The collisional stopping power for electron was derived by Bethe and Heitler using the Møller cross section [2] in the frame of quantum mechanics:

$$\begin{aligned} &\left(\tfrac{S}{\rho}\right)_{\text{col}} = \tfrac{2\pi r_e^2 m_0 c^2 N_{\text{A}} Z}{\beta^2 A}\left[\ln\left(\tfrac{E_k}{I}\right)^2 + \ln\left(1+\tfrac{\tau}{2}\right) + F^-(\tau) - \delta\right] \qquad [\text{MeV}\cdot\text{cm}^2/\text{g}] \\ &\text{with} \quad F^-(\tau) = (1-\beta^2)\left[1 + \tfrac{\tau^2}{8} - (2\tau+1)\cdot\ln(2)\right] \end{aligned} \tag{2.3}$$

Where

E_k is the classical kinetic energy of the electron,

N_{A} is the Avogadro number,

Z, A are respectively the atomic and mass numbers of the medium,

$m_o c^2$ is the electron rest mass energy,

β is the relativistic ratio of particle velocity v to the speed of light c,

τ is the electron kinetic energy normalized to $m_e c^2$,

δ is the density effect,

$F^-(\tau)$ is the electron function,

r_e is the classical electron radius,

I is the average minimum amount of energy that can be transferred to the absorber atom, estimated as $I(\text{eV}) \approx 11.5Z$.

The rate of bremsstrahlung production by electrons travelling through matter was derived from Bethe and Heitler, and it is given as follows:

$$\left(\frac{S}{\rho}\right)_{\text{rad}} = \frac{1}{137}\frac{r_e^2 N_{\text{A}} Z^2}{A}\left(E_k + m_0 c^2\right)\overline{B_{\text{rad}}} \qquad \left[\text{MeV}\cdot\text{cm}^2/\text{g}\right] \tag{2.4}$$

Where $\overline{B_{\text{rad}}}$ is a function of both Z and E_k, varying between 5.33 and 15 for electron kinetic energies in the range from 0.5 MeV to 100 MeV. Figure 2–2 page 20, shows mass collision stopping powers S_{col} and mass radiative stopping power S_{rad} for electrons in water, aluminum and lead.

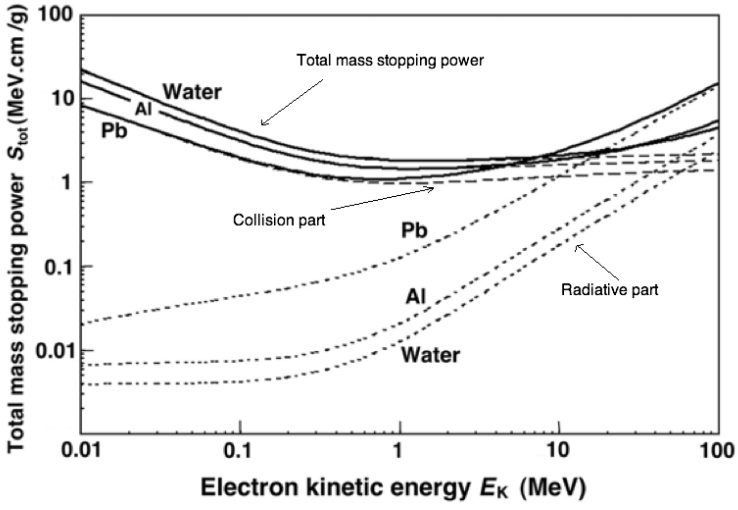

FIGURE 2–2 – Total mass stopping power S_{tot} for electrons in water, aluminum and lead against electron kinetic energy shown in *solid curves*. The mass collision and mass radiative stopping powers are shown with *dotted curves* for comparison. (Reproduced from Ervin.B. Podgorsak, Radiation Physics for medical Physicists, page 155) [1].

2.3.3 Restricted stopping power.

In the previous sections, we saw that when an electron suffers a collision with another electron, the latter one may receive enough energy to travel a significant distance away from the track of the primary electron and produce ionization and excitation on its own. These tracks are called « delta rays ». The mass collisional stopping power represents the rate of energy loss by the electron from all hard and soft collisions, including δ-rays produced from hard collision. Therefore, the use of mass stopping-power to estimate the dose may overestimate the energy deposited in a specific volume (unless CPE [5] exits). The notion of restricted stopping power has been introduced to evaluate the rate of energy loss by charged particles that includes all hard and soft collision but excludes the δ-rays with energies exceeding a cutoff value Δ. The choice for the threshold energy is typically 10 KeV. The restricted stopping power for electrons is calculated using the formalism of ICRU report Number 37 [3]:

$$\left(\frac{L}{\rho}\right)_{\Delta} = \frac{2\pi r_e^2 m_0 c^2 N_A Z}{\beta^2 A}\left[\ln\left(\frac{E_k}{I}\right)^2 + \ln\left(1+\frac{\tau}{2}\right) + G(\tau,\eta) - \delta\right] \quad [\mathrm{MeV}\cdot\mathrm{cm}^2/\mathrm{g}]$$
$$\text{with} \quad G(\tau,\eta) = 1-\beta^2 + \ln\left[4\eta\,(1-\eta)\right] + (1-\eta)^{-1} + (1-\beta^2)\left[\tfrac{1}{2}\tau^2\eta^2 + (2\tau+1)\ln(1-\tau)\right] \tag{2.5}$$

Where $\tau = \frac{E_k}{m_0 c^2}$, $\eta = \Delta/E_k$, and $G(\tau,\eta)$ is the « G-function » for electron. Figure 2–3 page 22 illustrates the unrestricted collision mass stopping power as well as the restricted collision mass stopping powers with $\Delta = 10$ KeV and $\Delta = 100$ KeV against kinetic energy E_{K} for electrons in carbon.

5. *CPE*: ***C**harged **P**article **E**quilibrium that exists in a volume V, if charged particles leaving this volume are replaced by an identical one of the same energy entering that volume V.*

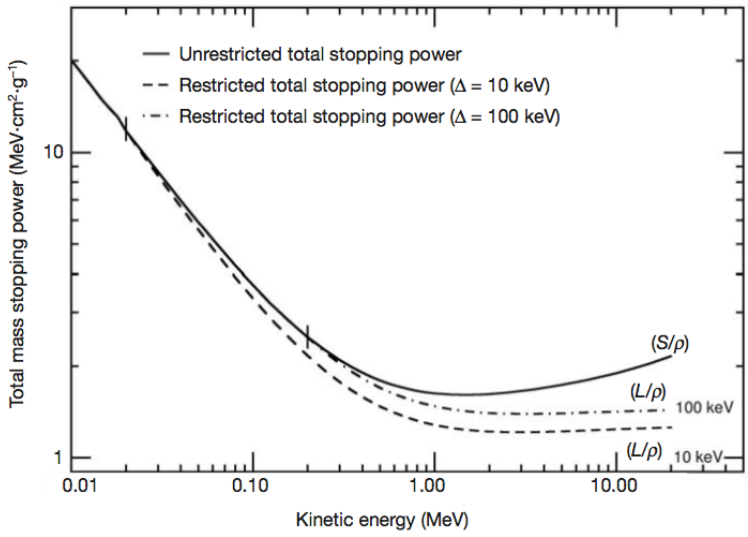

FIGURE 2–3 – Unrestricted and restricted ($\Delta = 10$ KeV and $\Delta = 100$ KeV) collision mass stopping powers for electrons in carbon against kinetic energy. Vertical lines indicate the points at which restricted and unrestricted mass stopping powers begin to diverge as the kinetic energy increases.(Reproduced from Ervin.B. Podgorsak, Radiation Physics for medical Physicists, page 163) [1].

2.3.4 Absorbed dose and KERMA.

The mean energy deposited indirectly or directly by ionizing radiation to a mass of medium m in a finite volume V is referred as absorbed dose. This can be expressed as:

$$D = \frac{d\bar{\epsilon}}{dm} \qquad [\text{J/Kg}] \text{ or } [\text{Gy}] \qquad (2.6)$$

The energy imparted ϵ corresponds to the difference between the energy of the electrons entering the volume to that leaving it, taking into account any mass-energy conversion occurring within the volume such as pair production and electron-positron annihilation. The absorbed dose is also related to the unrestricted mass collisional

stopping power through the differential electron fluence spectrum [6] as:

$$D = \int_0^{E_0} \frac{d\Phi(E)}{dE} \left(\frac{S}{\rho}\right)_{\text{coll}} \qquad \text{[J/Kg] or [Gy]} \qquad (2.7)$$

Note that as the electron travels through the medium, it deposits energy along its track, usually not at the same location as where it was set in motion. This notion is known as KERMA, acronym for **K**inetic **E**nergy **R**eleased per unit of **Ma**ss. This quantity applies only to indirectly ionizing radiation (photons, neutrons), contrary to the definition of absorbed dose. The KERMA is defined as the averaged energy transferred from indirectly ionizing radiation to directly ionizing radiation per unit of mass without concern to what happens after this transfer.

6. *The electron fluence corresponds to the number of electrons dN that crosses an area da at a right angle to the beam.*

References

[1] Ervin.B. Podgorsak. *Radiation Physics for Medical Physicists*, volume 1 edition. Springer Berlin Heidelberg New York., New York, 2005.

[2] C.Möller. Zur theories des durchgangs schneller elektronen durch materie. *Ann. Phys.*, 14 :468–577, 1932.

[3] ICRU. Stopping powers for electrons and positrons. PIRS 37, ICRU - International Commission on Radiation Units and Measurements, Washington, D.C, 1984.

Chapitre 3
ELECTRON BEAM DOSIMETRY

Contents

The purpose of this Chapter is to summarize the principles of electron beam dosimetry. Discussions on the basic characteristics of electron beams and on the measurement of absorbed dose with ionization chamber are included.

3.1 Electron beam characteristics.

3.1.1 General description of an electron depth-dose curve.

The most interesting characteristic of electron beam dosimetry is the shape of its depth-dose curve. Figure 3–1 page 26 shows a typical electron percentage depth dose curve. The curve shows a moderately flat plateau during the first few centimeters of water which results from the almost parallel path of the electrons as they enter the medium. As the electrons travel through deeper and deeper tissue, they transfer more and more energy to the media due to multiple scattering. Their paths become more and more oblique compared to their original direction. This consequently increases the

electron fluence and causes the dose to build up rapidly [1] , thus forming a moderate plateau. The maximum dose occurs at a depth where the electron paths become completely diffused. The dose buildup is followed by a rapid dose fall off as a result of electrons constantly loosing more energy. In addition, as the electrons interact with the different components of the accelerator, the air, and the patient, they produce bremsstrahlung photons that will cause a tail in the depth dose curve at larger depth. This contamination represents less than 1% to 4% for 4 MeV to 20 MeV electron beam respectively. As the electrons enter the medium, they immediately start to transfer energy in comparison to photons that travel deeper into the tissue before setting up in motion an electron that will initiate the energy absorption process. Therefore the surface dose is much higher for electron beams than for photon beam. So the combination of high surface dose combined with a rapid fall off makes electron beam treatments very useful for superficial tumors.

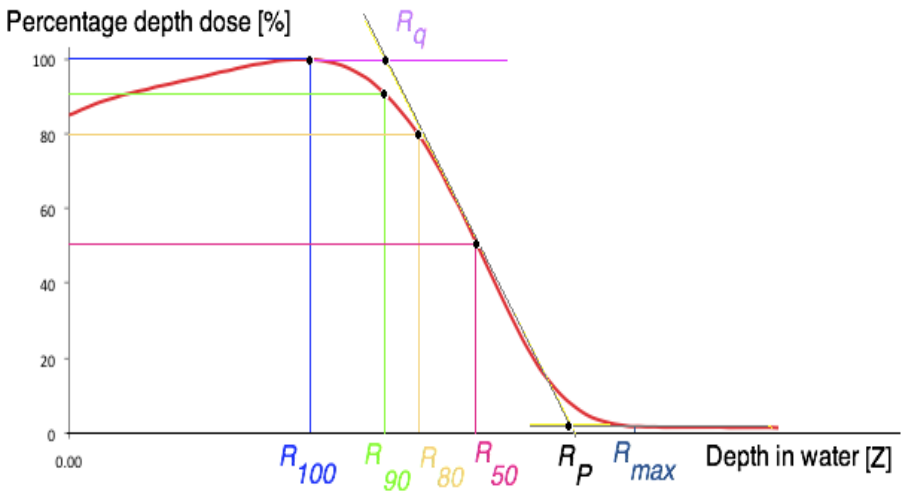

FIGURE 3–1 – *A typical electron central axis percentage depth dose curve, illustrating important specific depths.*

1. *As compared to photon beam buildup region.*

3.1.2 Electron range definitions.

As an electron beam impinges matter, electrons transfer a fraction of their kinetic energy to the medium, change direction and produce bremsstrahlung photons. Eventually, all electrons of the initial beam will reach a point where all their energy will be dissipated into the medium and the electrons will come to rest. The depth beyond which no initial electrons are present is called the practical range R_{P}. Even if an electron loses fraction of its energy with every atom it encounters, it is more convenient macroscopically to think as if the electron is loosing its kinetic energy continuously. This process is referred as the continuous slowing down approximation (CSDA). Therefore, the CSDA range (R_{CSDA}) of an electron can be viewed as an integration along the actual path of the electron and can be mathematically expressed as:

$$R_{\mathrm{CSDA}} = \int_{E_0}^{E} \left(\frac{S}{\rho}\right)_{Tot}^{-1} dE \qquad \left[\frac{\mathrm{g}}{\mathrm{cm}^2}\right] \text{ or } [\mathrm{cm}] \tag{3.1}$$

Where E_0 represents the initial electron kinetic energy, i.e. the energy as it enters the phantom, and $\left(\frac{S}{\rho}\right)_{\mathrm{Tot}}^{-1}$ is the inverse total stopping power. Table 3–1 page 27 tabulates various electron ranges in water over a large range of electron energies.

TABLE 3–1 – *Electron ranges in water [1].*

Electron Energy [KeV]	Range R $[\frac{\mathrm{g}}{\mathrm{cm}^2}]$	Electron Energy [MeV]	Range R $[\frac{\mathrm{g}}{\mathrm{cm}^2}]$
10	0.0003	1	0.4359
20	0.0009	4	2.019
40	0.0029	6	3.052
80	0.0098	9	4.506
100	0.0143	10	0.0404
200	0.0447	20	0.0826
800	0.3294		

Other specific depths are also used to characterize an electron beam. For instance, the depths at which the electron percentage depth dose (PDD) curve falls off

to 50%, to 80% and to 90% are respectively referred to R_{50}, R_{80}, and R_{90}. According to ICRU report 21 [1], the variation in dose delivery to the tumor volume should be within 5% of the prescribed dose. Hence, only the dose from the depth of maximum dose up to the 90% dose level in the electron PDD should be used to cover the treatment target. R_{90} should coincide with the distal treatment margin and is often defined as the therapeutic range. Therefore, the 90% dose level makes a perfect candidate to match measured with calculated dose. The maximum distance of penetration in the absorbing medium is referred to as the maximum range $R_{\max}$ and corresponds to the distance where the tail of the PDD meets the bremsstrahlung tail. R_{p} is the practical range and it is defined as the distance where the tangent at the steepest point of the fall-off portion of the electron PDD curve intersects the bremsstrahlung tail. The depth R_{q} is defined as the depth where the tangent through the dose inflection point intersects the maximum dose level. Finally, the depth where the electron beam deposits the maximum energy is R_{100} (or $Z_{\max}$). An important aspect of the electron PDD is that the depth of dose maximum is a result of machine head, accessories, geometries and characteristics.

3.1.3 Electron beam energy specification.

The main characteristic of an electron beam PDD is the sharp dose fall-off with depth. The depth of this fall-off is a function of initial beam energy, and it is therefore necessary to characterize the initial electron beam energy accurately. Figure 3–2 page 29 illustrates the energy spectrum of the electron beam as it leaves the accelerator.

E_{a} is the energy at which the machine accelerates the electron and is in general characterized by a very narrow energy spread. The pencil beam diameter is usually around 3 mm. As the beam leaves the accelerator exit window, its energy spectrum spreads as it goes through the various components of the linac treatment head (scattering foil, monitor chamber, jaws, air, ...). $\overline{E}_0$ is the mean electron beam energy at the

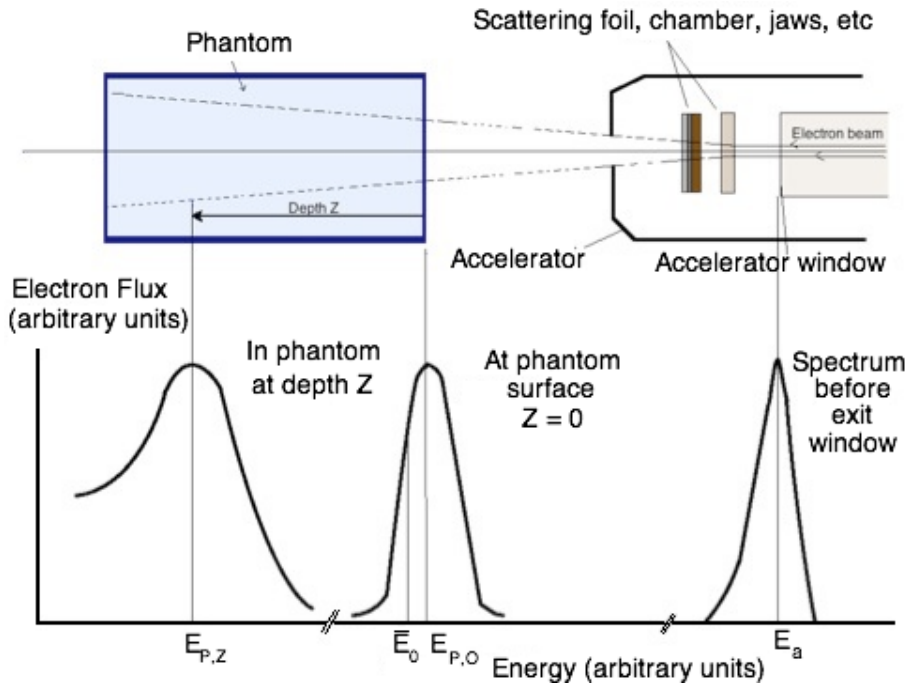

FIGURE 3–2 – *Distribution of the electron beam energy spectrum as it travels through the treatment head and the phantom.(Adapted from ICRU report 21 [1])*

phantom surface. The energy spectrum will spread even more as it goes though the phantom. Determining the electron beam energy is challenging and in clinical practice, it is characterized at the phantom surface and several methods can be used to evaluate it. These include: (1) measurement of Čerenkov radiation (see Section 2.3.1 page 16) radiation threshold, (2) measurements of the minimum energy to initiate nuclear reactions and (3) the method of ranges. The first two methods are technically difficult and time-consuming whereas the practical range method is straightforward and easy to use. Therefore the range method was chosen as the principal method in this thesis to determine electron beam energies at the phantom surface.

As illustrated in Figure 3–2 page 29, the electron beam energy at the phantom surface is characterized by a spectrum with a peak energy at $E_{\mathrm{P},0}$. This energy corresponds to the most probable electron energy at the exit window. The Nordic Association of Clinical Physics [2] (NACP -1980) recommends the following empirical

formula to determine this energy:

$$E_{\mathrm{P},0} = C_1 + C_2 \times R_{\mathrm{P}} + C_3 \times R_{\mathrm{P}}^2 \qquad [\mathrm{MeV}] \tag{3.2}$$

Where R_{P} is the practical range in MeV defined earlier, and C_1, C_2 and C_3 are constants defined by the NACP [2] and the ICRU [1] as follows: $C_1 = 0.22$ MeV; $C_2 = 1.98$ MeV$\cdot$ cm^{-2}; $C_3 = 0.0025$ MeV$\cdot$ cm^{-2}.

Analysis of various depth dose curves along the central axis for several accelerators in combination with Monte-Carlo dose calculations shows that the mean energy of an electron beam at the phantom surface is directly proportional to the depth at which the dose falls to 50% [1–5]. This is mathematically expressed as:

$$\overline{E_0} = C_4 \times R_{50} \qquad [\mathrm{MeV}] \tag{3.3}$$

Where R_{50} is the depth at which the dose is 50% of the maximum dose. $\overline{E_0}$ is the mean energy at the water surface (illustrated in Figure 3–2 page 29) and C_4 is the constant of proportionality. According to AAPM [6] task-group 21, the value of C_4 is evaluated to be 2.33 MeV/cm in water.

Another important parameter is the mean energy at depth Z in a water phantom. Harder [7] has demonstrated that the spectral energy $E_{\mathrm{P,Z}}$ at depth Z in a water phantom (illustrated in Figure 3–2 page 29) is linearly expressed as:

$$E_{\mathrm{P,Z}} = E_{\mathrm{P},0} \times \left(1 - \frac{\mathrm{Z}}{R_{\mathrm{P}}}\right) \qquad [\mathrm{MeV}] \tag{3.4}$$

Which can be approximated as follows:

$$\overline{E_{\mathrm{Z}}} = \overline{E_0} \times \left(1 - \frac{\mathrm{Z}}{R_{\mathrm{P}}}\right) \qquad [\mathrm{MeV}] \tag{3.5}$$

This relation is also known as the Harder equation.

3.2 Dosimetry measurements principle and methods.

3.2.1 Dose measurements with ionization chambers.

The measurement and/or calculation of absorbed dose, fluence, air $KERMA$, equivalent dose or any other physical dose related quantity is referred to as *radiation dosimetry*. Dosimetric measurements are performed with devices called radiation dosimeters. There is not a single universal technique and/or radiation dosimeter applicable for all possible photon or electron beams measurements. For example, an ionization chamber is an excellent dosimeter to determine beam output, however, it is not suitable for surface dose measurements.

There are two types of dosimeters: *absolute dosimeters*, capables of determining the dose directly without requiring calibration in a know field of radiation, and *relative dosimeters* which require a known radiation field as a reference. Ionization chambers can be used as relative or absolute dosimeters and they are the most commonly used dosimeters for photon and electron beams. They come in different designs: cylindrical (or thimble), spherical and parallel-plate (or end window) (see Figure 3–3 page 32). Generally, cylindrical ionization chambers are mainly used for photon beams and high-energy electron beams, whereas parallel-plate (PP) chambers are recommended for low energy electron beams below 12 MeV. The principle and design of a cylindrical ionization chamber is based on the fact that a central electrode will collect the ions produced as the result of interactions between the air molecules with the primary and secondary electrons. These electrons were set in motion by the beam crossing the chamber sensitive volume. The design of the dosimeter is also optimized to minimize leakage. For instance, the collecting electrode and the chamber walls are separated with an insulator. To further reduce leakage, guard electrodes are set-up to intercept leakage current and direct it to the ground. It is also important to ensure that for an unsealed ionization chamber, the measured signal is corrected for temperature, pressure, and humidity to account for the change of air mass in the sensitive volume.

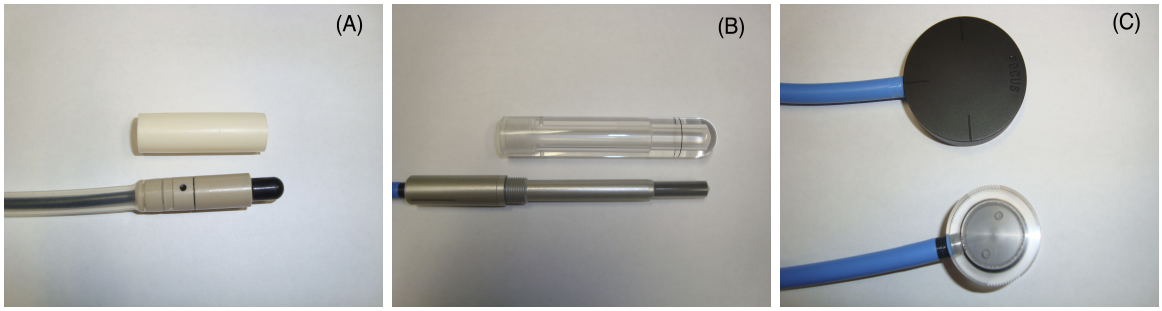

FIGURE 3–3 – *Example of typical ionization chambers used in radiotherapy*:
(A) *cylindrical ionization chambers ;*
(B) *Farmer-type cylindrical chamber with a Cobalt-60 buildup cap ;*
(C) *parallel plate electron beam ionization chamber.*

Most of the measurements performed in this work were done with a Wellhöfer IC-10 (Scanditronix-Wellhöfer, Schwarzenbruck, Germany) cylindrical ionization chamber. This cylindrical chamber is basically a cavity ionization chamber that consists of a solid envelope surrounding a gas, such as air, in which the ions created by radiation are collected on a collecting electrode while applying an applied electric field. Ionization chambers are generally a good choice for determining the relative radiation dose distribution within a medium, in particular along the central axis of the beam. However, for measurements near the surface, i.e. in the build-up region, parallel-plate (PP) chambers are most suitable due to their thin entrance window that yields betters spacial resolutions in the direction perpendicular to the beam. Gafchromic® EBT films (International Speciality Products, NJ, USA) are also a good candidate to measure dose deposition in the build-up region or to measure dose distribution for small field sizes. More details on Gafchromic® EBT films in the context of our work will be given in Chapter 5.

3.2.2 Electron beam depth-dose measurements.

Dosimetry techniques vary for different types of beams. For example, the dosimetry of electrons is quite different than that of photons. As a photon beam enters

a medium, electrons are produced thought various processes (see Section 2.2 page 12) and the beam has essentially the same energy spectrum at any point within the medium. However, with an electron beam, the electron's energy constantly decreases with depth, where the maximum is deposited near the surface and the minimum is deposited at depth close to the electron range. It has been shown by Monte Carlo simulations that the water/air stopping power ratio $\left(\frac{S}{\rho}\right)_{\text{air}}^{\text{water}}$ for monoenergetic electron beams varies as a function of depth, hence as a function of energy. However, stopping power ratios $\left(\frac{S}{\rho}\right)_{\text{air}}^{\text{water}}$ for photon beams is almost constant beyond the depth of maximum dose. Therefore, determining the dose for an electron beam requires additional considerations as the energy spectrum changes with depth.

Using an ionization chamber to scan the electron beam central axis, a depth-ionization curve is obtained. To convert it to a central-axis depth-dose curve, one needs to correct the ionization data at each depth with the stopping power ratio. The value of the stopping power ratio (water/air) can be approximated by the Burns equation [8]:

$$\left(\frac{L}{\rho}\right)_{\text{air}}^{\text{water}}(Z, R_{50}) = \frac{a + b\left(\ln\left(R_{50}\right)\right) + c\left(\ln\left(R_{50}\right)^2\right) + d\left(\frac{Z}{R_{50}}\right)}{1 + e\left(\ln\left(R_{50}\right)\right) + f\left(\ln\left(R_{50}\right)^2\right) + g\left(\ln\left(R_{50}\right)^3\right) + h\left(\frac{Z}{R_{50}}\right)} \quad (3.6)$$

Where a = 1.0752, b = -0.50876, c = 0.088670, d = -0.08402, e = -0.42806, f = 0.064627, g = 0.003085 and h = -0.2460 and R_{50} and Z are in units of cm.

3.3 Dosimetric measurements in water phantom.

The main goal of radiation dosimetry is to determine the dose distribution in the patient. Therefore, it is essential to first determine the 3 dimensional dose distribution in water for each clinically available beam. This is usually achieved in water-equivalent material. For dosimetric measurements of photon and electron beams, ICRU report

24 (ICRU, 1976) and report 21 (ICRU, 1972) have recommended using a water phantom as a reference medium. Water is universally recognized as the most appropriate substitute material to mimic human tissues since its properties closely approximate the radiation absorption and scattering effects of muscle and other soft tissues. Determination of size and composition of internal organs is complicated and assuming that the whole patient is water equivalent is a good first order approximation.

When measuring dosimetric quantities in a phantom, liquid water will pose a problem to non-waterproof detectors. For this reason, water equivalent materials are often used for dosimetric measurements. Such materials include: polystyrene, lucite, A-150 tissue equivalent plastic, Solid Water® RMI-457 (Gammex RMI, Middleton, WI), Plastic Water, etc... They have been developed as substitutes for liquid water by mimicking the properties of water in term of three parameters: (1) the effective atomic number, (2) the number of electrons per gram and (3) the mass density. For photon dosimetry, a phantom is said to be water equivalent if the mass stopping power, the mass-energy absorption coefficient and the mass scattering power equate that of water. Whereas for electron beams, linear stopping power and linear scattering power of the equivalent material and that of water must be the same. In practice, there is no ideal water-equivalent material and phantom materials used for photon beams are also generally used for electron beams. One of the most widely used substitute of liquid water for radiotherapy photon and electron beams measurements is Solid Water® (developed by Constantinou [9]). Solid Water® is a registered trademark of Gammex RMI.

References

[1] ICRU. Radiation dosimetry : Electron beams with energies between 1 and 50 MeV. PIRS 35, ICRU - International Commission on Radiation Units and Measurements, 1984. Bethesda, Maryland.

[2] NACP. Procedures in external radiation therapy dosimetry with electron and photon beams with maximum energies between 1 and 50 MeV. Acta Radiol. 19 :55, Nordic Association of Clinical Physics (NACP)., 1980.

[3] NACP. Electrons beams with mean energies at the phantom surface below 15 MeV. Acta Radiol. Oncol. Rad. Phys 20 402-415, Nordic Association of Clinical Physics (NACP)., 1981.

[4] IAEA. Absorbed dose determination in external beam radiotherapy - an international code of practice for dosimetry based on standards of absorbed dose to water. Technical Report Technical report Series No. 398, IAEA - International Atomic Energy Agency., 2000. Sponsored by the IAEA, WHO, PAHO and ESTRO.

[5] IAEA. The use of Plane Parallel Ionization Chambers in High Energy Electron and Photon Beams : An International Code of Practice for Dosimetry. Technical Report Technical report Series No. 381, IAEA - International Atomic Energy Agency Vienna, 1997. Sponsored by the IAEA, WHO, PAHO and ESTRO.

[6] Briesmeister J F. A protocol for the determination of absorbed dose from high energy photon and electron beams. Technical Report Task group Number 21, AAPM - American Association of Physicists in Medicine., 1983.

[7] Harder D. Energiespectren scgneller elecktronen in verschiedenen tiefen. in : Monstreux, zuppinger a, poretti g, eds. symposium on high-energy electrons. *Springer-Verlag - Berlin*, 26 :260, 1965.

[8] G. X. DING D.T. BURNS and W. O. Rogers. R_{50} as a beam quality specifier for selecting stopping-power ratios and reference depths for electron dosimetry. *Med. Phys.*, 23 :383–388, 1996.

[9] Constantinou C Attix FH Paliwal BR. A SolidWater® phantom material for radiotherapy x-ray and gamma-ray beam calibrations. *Phs. Med. Biol.*, 9 :436–41, 1982.

Chapitre 4
MONTE CARLO METHOD FOR RADIATION TRANSPORT AND DOSE CALCULATIONS

Contents

In this Chapter, the application of the Monte Carlo method applied to radiation transport will be presented. Although the technique can be applied to the transport of neutrons and heavy particles, emphasis will be given to photons and electrons that are relevant to this work. Discussions in this Chapter will focus on the electron gamma shower (EGS) [1] which is recognized as the reference Monte Carlo transport computer code in the medical physics field.

4.1 The Monte Carlo techniques for radiation transport.

Calculating the dose distribution within a patient with good accuracy is a difficult task. According to ICRU report 21 [2], the radiation dose delivered to a patient by a clinical electron beam should be within 5% of the prescribed dose. This 5% includes all uncertainties associated with the radiotherapy treatment such as machine calibration (up to 2%), patient set-up, uncertainty related to the patient motion during the treatment, imaging/diagnostics uncertainties and uncertainties related to the treatment planning (TP) dose calculation. Over the past few years, important work has been done to obtain better electron TP algorithms to accurately calculate

dose deposition in a patient with minimum discrepancy to measurements. Current commercial TPS use the Fermi-Eyges pencil beam model and do not systematically provide acceptable agreement with measurements. Dose calculations using the Mote Carlo (MC) method is currently the reference method in radiation physics. It has been demonstrated that MC is more accurate for dose calculations in situation where heterogeneous media and complex geometries occur [3–5]. The first use of Monte Carlo principles in medical physics started in 1976 [6, 7]. At this time, the applications were very limited due to the lack of computing power. However, with the fast development of computer technology, the use of Monte Carlo techniques in radiation transport has became a gold standard. Several Monte Carlo code distributions have been developed and are currently applied for research in radiation physics. A partial list of these distributions includes: GEANT4 [8] (**GE**ometry **AN**d **T**racking), Fluka [9] (**FLU**ktuierende **KA**skade), PENELOPPE [10] (**PEN**etration and **E**nergy **Lo**ss of **P**osition and **E**lectron), MCNP/ MCNPX [11] (**M**onte **C**arlo **N-P**article-e**X**tended), ETRAN [12] (**E**lectron **Tran**sport), MCEF [13] and EGS [1, 14] (**E**lectron **G**amma **S**hower) developed by the National Research Council (NRC) of Canada. All these codes differ in the way they simulate the transport of a particle trough matter, the type of particle simulated, the interactions processes, cross sections involved, the variance reduction techniques used, the program architecture and design, the efficiency of the algorithm, etc... However, they all have one point in common: they assume that the particles interact with matter only, and not with each other. Some codes have shown to be more robust than others, and some have yielded very promising results such the EGSnrc code system that will be discussed in more details.

4.2 Principle of Monte Carlo techniques.

The Monte Carlo method applied to radiation physics is a statistical based approach to simulate the transport of each individual particle by the use of random number generator. Random variables, generated by a random number generator (RNG), are sampled from probability distributions functions (PDFs), which describe the theoretical interactions processes of photons, electrons and positrons with matter. The simulation of photons and electrons transport is described below.

As described in Chapter 1, when a photon travels through matter, it may undergo various processes: *Rayleigh*, *photoelectric*, *Compton* or *pair production* effects. Monte Carlo simulates the transport interaction of photons by sampling probability distributions using random numbers. Basically, the initial direction, starting position and energy of a photon are sampled from distributions of incident photons. Then the distance to the next interaction point in the medium is randomly determined by sampling a function of photon's mean free paths. The type of interaction that occurs after the photon has traveled a distance l is sampled from a cross section probability distribution. If the photon energy is larger that a cut-off value ($PCUT$), the distance l to the next site is sampled, otherwise the simulation for this particular photon is terminated. Each photon is transported following that method until it leaves the volume of interest or until it has deposited all its energy into the medium. This is called a particle history.

The above algorithm for simulating the transport of electrons through matter cannot be applied since the slowing down process of electrons implies a very large number of electrons interactions as compared to photon transport. Using step-by-step or direct simulation of all physical interactions would make the simulation unacceptably inefficient and complex. Therefore the transport of electron adds a new dimension to MC calculations and has motivated physicists to introduce the condensed history (CH) technique. This idea was first introduced in 1962 by Berger [15, 16]. Instead

of applying a full electron transport algorithm, interactions are grouped (condensed) together. In this approach, the large number of electron collisions are broken into short electron steps. This technique is very adequate since during a single electron-particle interaction only a fraction of the electron's kinetic energy is transferred to the medium and the change of direction and energy of the particle is minimal.

4.3 Radiation transport with the EGS algorithm.

4.3.1 Introduction to electron gamma shower (EGS).

As mentioned previously, different Monte Carlo codes are available to simulate particle transport in any medium. Some codes were shown to be very good to model particle transport in the energy range by which medical physics is concerned; one of them is the Electron Gamma Shower (*EGS*). *EGS* is the most widely used code in the field of medical physics and has been chosen for our work. When it was introduced in 1978, *EGS* was primarily used for applications in high energy physics but rapidly evolved to *EGS4* [17], a version that is more applicable to medical physics. It was later updated to *EGSnrc* [1, 14, 16, 18] with further improvements such as more accurate electron transport algorithm: *PRESTA II*. The concept of energy thresholds was also introduced. The total electron energy below which electrons are not transported is referred to as *ECUT*. Whereas *PCUT*, corresponds to the photon energy below which the photon transport is stopped. *EGSnrc* also includes *AE* and *AP* threshold values, and cutoffs values for the collisional and radiative part of the restricted stopping powers respectively. *AE* can be seen as being the total electron energy above which delta-rays are generated and *AP* as the photon energy above which bremsstrahlung photons are created. Therefore, lowering *AP* and *AE* cutoffs would improve calculation accuracy at the expense of increasing computing time. Other concepts are also incorporated into *EGSnrc* to ensure that electrons are accurately transported in the neighborhood or across boundaries of different materials. This is achieved through the

use of a boundary-crossing algorithm (BCA). If *EXACT BCA* is activated, EGSnrc will make particles cross boundaries in a single elastic scattering mode, such that the distance from the boundary at which the algorithm will go into single scattering mode is determined by the *Skin depth* of *BCA*. Otherwise the standard *PRESTA-I BCA* algorithm is used. In EGSnrc, a number of routines and subroutines are used to handle the geometry (*HOWFAR* and *HOWNEAR*), to manage the particle scoring (*AUSGAB*), to read the media cross-section from a *PEGS4* [19] files (*HATCH*), to generate a full and complete history about each and every particles (*SHOWER*). All theses routines and subroutines are part of the EGSnrc code, and EGSnrc is also the base of higher level code such as *BEAMnrc* [20] and *DOSXYZnrc* [21].

4.3.2 BEAMnrc code for simulating linear medical accelerator.

Developed through the OMEGA project [22], BEAM [23], later updated to BEAMnrc [20], is a Monte Carlo Code built on the Electron-Gamma-Shower Code System and can be used to simulate the transport of radiation through a virtual linear accelerator customizable model. The BEAMnrc code offers a collection of component modules (CM) which simulates specific typical geometries of various parts of an accelerator head. The geometry, composition, location and dimensions of each CM are built using the linac manufacturer specifications. Each CM is designed to fill a known space perpendicular to the beam's central axis. CMs cannot overlap with each other. The gaps between CMs are filled with any specific material, usually air or vacuum. The linear accelerator is then built by stacking all the different component modules. The simulations can benefit from some variance reduction techniques selectable by the user. These include: range rejection techniques, photon forcing, uniform and selective bremsstrahlung splitting. An other important feature of BEAMnrc is the possibility to save phase-space files. A phase-space file contains information about each and every particle crossing a selected simulation plane. The use of phase-space

files and its impact on our current work will be explained in the next Chapter.

4.3.3 Dose calculations using DOSXYZnrc.

A phase-space file created by BEAMnrc can be used as an input to a DOSXYZnrc simulation. DOSXYZnrc is an EGSnrc source code that allows the user to score dose into a three-dimensional voxel based geometry.patient. The dimension and density of any single voxel is arbitrary and can be set by the user. It can also be created from a patient CT [1] scan information. As BEAMnrc, DOSXYZnrc offers different options. For instance *HOWFARLESS* is an option used to increase the efficiency of dose calculations in homogeneous phantoms. Various parameters are available within DOSXYZnrc, and those relevant for our project will be detailed in the next Chapter.

1. Computerized Tomography. Imaging technique using ionization radiation that permits non-invasive depiction of body structures

References

[1] Kawrakov I and Rogers D W O. EGSnrc / BEAMnrc / DOSXYZnrc. EGS electron gamma source. Pirs, NRCC - Canada Ottawa - National Research Council., 2003.

[2] ICRU. Radiation dosimetry : Electrons with initial energies between 1 and 50 MeV. PIRS 21, ICRU - International Commission on Radiation Units and Measurements, 1972. Bethesda, Maryland.

[3] E. Mah J. Antolak J. W. Scrimger and J. J. Battista. Experimental evaluation of a 2D and 3D electron pencil beam algorithm. *Phys. Med. Biol.*, 34 :1179–1194, 1989.

[4] J. Cygler J. J. Battista J. W Scrimger E. Mah and J. Antolak. Electron dose distributions in experimental phantoms ; a comparison with 2D pencil beam code. *Phs. Med. Biol.*, 32 :1073–1086, 1987.

[5] K. R. Shortt, C. K. Ross, A. F. Bielajew, and D. W. O Rogers. Electron beam dose distributions near standard inhomogeneities. *Phs. Med. Biol.*, 31 :235–249, 1986.

[6] D E Reaside. Monte carlo principles and applications. *Med. Phys. Biol.*, 21 :181–197, 1976.

[7] P Andreo. Monte Carlo techniques in medical radiation physics. *Med. Phys.*, 36 :861–920, 1991.

[8] CERN. GEANT - GEometry ANd TRacking. Technical report, CERN - European Organization for Nuclear Research., 1982.

[9] INFN & CERN. FLUKA - (FLUktuierende KAskade). Technical report, Italian National Institute for Nuclear Physics (INFN) and by the European Organization for Nuclear Research (CERN)., 1982.

[10] UB. PENELOPPE - PENetration and energy LOss of Positron and Electron. Technical report, Universitad de Barcelona, 1982.

[11] Briesmeister J F. MCNP - a general Monte Carlo N-particle transport code version 4C. Technical Report LA-12625-M, Los Alamos Natl. Lab., 2000.

[12] Berger and Seltzer. ETRAN - electron transport. Technical report, National Institute of Standars and Technology, 1968.

[13] Nordic Association of Clinical Physics NACP Andreo et al. MCEF source code - Monte Carlo for Evaporation-Fission calculations. Technical report, University of Zaragoza, Spain Karolinska Institute-University of Stockholm, Sweden, Andres, 1988.

[14] Kawrakov I and Rogers D W O. The EGSnrc code system : Monte Carlo simulation of electron and photon transport. Pirs-701, NRCC - Canada Ottawa - National Research Council., 2003.

[15] M.J Berger. Monte Carlo calculation of the penetration and diffusion of fast charged particles. *Nucl. Instrum. Methods Phys. Res.*, 134 :135–215, 1963.

[16] Kawrakow I. Accurate condensed history Monte Carlo simulation of electron transport II. application to ion chamber response simulation. *Med. Phys.*, 27 :499–513, 2000.

[17] Rogers D W O Nelson W R and Hirayama H. The EGS4 code system. *Stanford Linear Accelerator Center Report - SLAC*, 1 :265, 1985.

[18] Kawrakov I and Rogers D W O. The EGSnrc system status report from advanced Monte Carlo for radiation physics, particle transport simulation and applications. In *proceedings of the Monte Carlo 2000 Conference*, Lisbon, October 2000. NRCC - Canada Ottawa - National Research Council., Springer.

[19] W.R. Nelson. PEGS4 : datasets for different media - Course on Electron and Photon Transport using the EGS4 Monte Carlo System. In UK National Physical Laboratory, Teddington, editor, *EGS4 : datasets for different media*, volume Lecture 9. Stanford Linear Accelerator Center, September 1989.

[20] Rogers DWO, Ma Ding, GX Walter, Sheikh-Bagheri and Zhang GC. BEAMnrc users manaual. Pirs 509a (rev f), NRCC - Canada Ottawa - National Research Council., 2001.

[21] Walters B, Kawrakow I, and Rogers D W O. DOSXYZnrc users manual. PIRS 794revB, NRCC, 2004.

[22] Mackie T R. Application of the Monte Carlo method in radiation therapy. *The dosimetry of Ionization Radiation*, 3 :541 – 620, 1990.

[23] Rogers D W O, Faddegon B A, Ding G X, Ma C M, Wei J, and Mackie T R. BEAM : A Monte Carlo code to simulate radiotherapy treatment units. *Med. Phys.*, 22 :503–524, 1995.

Chapitre 5
DOSIMETRIC EQUIPMENTS, MATERIALS AND MONTE CARLO METHODS

Contents

The first part of this Chapter enumerates the various measuring tools, equipments and setups used to collect the data. Our MC commissioning procedure includes the measurements of percentage depth dose curves and transverse dose profiles at various depths of clinical interest. The second part will describe the geometry and the transport parameters that were used to simulate a Clinac 21-EX treatment head using BEAMnrc and a water phantom using DOSXYZnrc.

5.1 Experimental set-up for Electron dosimetric measurements.

5.1.1 Ionization chambers.

Most of the measurements for this work were performed with a waterproof Scanditronix Wellhöfer (FDA-Registered Company, Wellhöfer, Schwarzenbruk, Germany) IC-10 cylindrical ionization chamber IC-10. Ionization chambers were chosen because of their stability, high precision, availability, ease of use, and high reproducibility for dose measurements. Table 5–1 page 45 tabulates various characteristics of the Wellhöfer cylindrical ionization chamber. Data were collected at the Jewish General Hospital and at the Montreal General Hospital on two distinct medical accelerators: two Varian Clinac 21-EX.

TABLE 5–1 – *Characteristics of the Wellhöfer IC-10 (Scanditronix Wellhöfer) cylindrical ionization chamber (as stated by the manufacturer [1])*

Ionization Chamber Type	Cavity Volume [cm^3]	Cavity length [mm]	Cavity Radius [mm]	Wall Material	Wall Thickness [$\frac{g}{cm^2}$]	Central electrode material	Waterproof
Wellhöfer IC-10	0.14	6.3	3.0	C-552	0.068	C-552	Yes

An IC-10 Scanditronix Wellhöfer reference chamber was also set-up in the electron field in order to compensate for fluctuations of the accelerator output. The ratio of the two signals was used as the ionization reading. Both chambers were connected to a specific electrometer in order to measure the ionization charge. A high potential of 300 Volts was supplied between the ionization chamber electrodes. Irradiation to the chamber's stem and cable by high-speed electron often yields to the production of unwanted secondary electron. Therefore, to minimize the effect of spurious ionization current, stem and cable were led away from the radiation field while performing measurements.

5.1.2 Phantoms.

An IBA Blue phantom (IBA Dosimetry America, Bartlett, TN, USA) water tank was used to perform our dose measurements for the regular cutouts (Figure 5–1 page 46). The IBA tank is equipped with direct current (DC) motors and timing belts to ensure smooth, accurate and precise motion of the detector through the water without perturbing the liquid surface. The control software of this tank offers both a step by step and a continuous acquisition mode. It can be controlled remotely from the linac control room. The engraved crosshairs help to correctly align the tank with respect to the linac and the room lasers. Specifications of the IBA Blue water phantom are given in table 5–2 page 46.

FIGURE 5–1 – *Photo of an IBA Blue Phantom water tank with lift table [2].*

TABLE 5–2 – *Technical specifications of the IBA Blue water phantom (as stated by the manufacturer) [2].*

Scanning Volume :	480 mm (L) × 480 mm (W) × 410 mm (H)
Scanning speed (continuous) :	up to 15 mm/s
Position reproducibility :	min. 0.1 mm
Position accuracy :	± 0.5 mm
Approximation volume :	200 L
Wall material :	acrylic (plexiglass)
Water tank exterior dimension :	675 mm (L) × 645 mm (W) × 560 mm (H)
Weight :	46 Kg

5.1.3 Electron applicators and cutouts.

As explained in Chapter 1, electron beams need to be collimated near to the patient's skin as the beam edges become less defined as the electrons scatter in air. This is achieved by the use of applicators (also known as cones), specially designed for electron therapy. The Varian Clinac 21-EX comes with different electron applicators sizes: (6×6) cm^2, (10×10) cm^2, (15×15) cm^2, (20×20) cm^2 and (25×25) cm^2 (see Figure 1–3 in Chapter 1 page 7). To further collimate the beam to the shape of the tumor, and hence to minimize the dose to the surrounding tissues, special dedicated metal plates (or electron beam cutouts) of different sizes and shapes are inserted at the end of the applicator. For our work, six different cutouts were used to validate our model (see Figure 5–2 page 48). These cutouts are made of Cerrobend®, a low melting point (70^0 C) alloy made of bismuth (50% by weight), lead (26.7%), tin (13.3%) and cadmium (10%). The required shielding thickness of the electron cutouts should be approximately equal to the maximum range in Cerrobend® of the highest electron energy beam, 20 MeV in our work. Therefore, the cutout's thickness for all was 1.8 cm.

TABLE 5–3 – *Corresponding jaw's opening for clinical electron beam using specific applicators. All measurements are in centimeters [3].*

Energy Applicator Code	4,6,9 MeV	12 MeV	15,16 MeV	18,20,22 MeV
10×10	20×20	14×14	14×14	14×14
15×15	20×20	17×17	17×17	17×17
20×20	25×25	25×25	23×23	22×22
25×25	30×30	30×30	28×28	27×27

For each cone there is an associated jaw setting that is generally larger that the field size defined by the electron beam cone. In order to minimize the variation of dose rate and output factor with field size, associated jaws opening for each applicators and beam energy were used (see Table 5–3 page 47). For all cutouts, excepting the

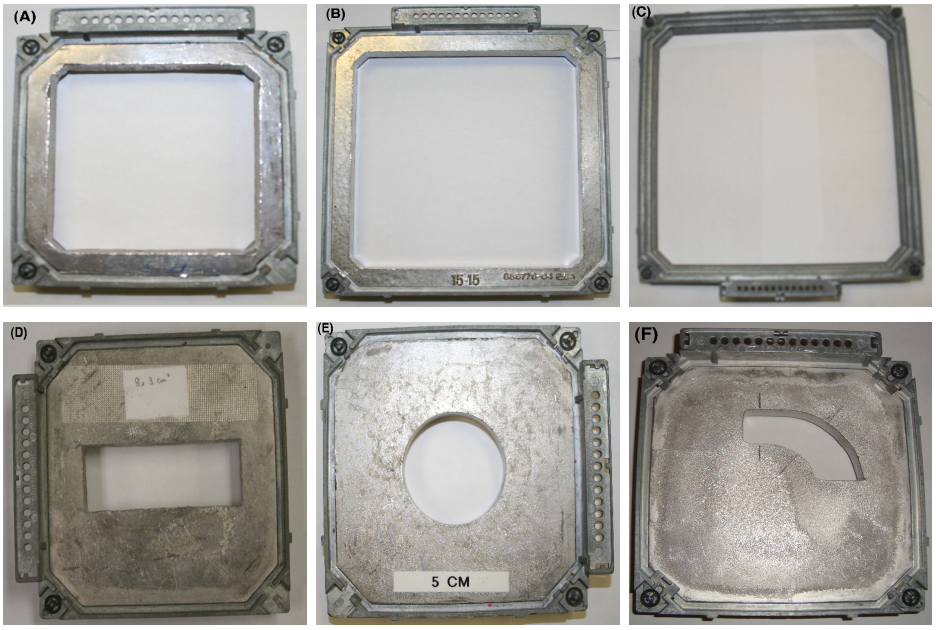

FIGURE 5–2 – *Cutouts used to validate our electron beam model*:
(A) *(10×10) cm² square cutout;* ***(D)*** *(8×3) cm² rectangular cutout;*
(B) *(15×15) cm² square cutout;* ***(E)*** *circular cutout of diameter 5 cm;*
(C) *(20×20) cm² square cutout;* ***(F)*** *quarter doughnut-shaped irregular cutout.*

irregular one, percentage depth dose curves were measured in water along the central beam axis (i.e. at the center of each Cerrobend® insert) and profiles were measured at the associated depths of maximum dose. In order to validate small irregular fields, a special shaped Cerrobend® insert was constructed to fit at the bottom of a (10×10) cm² applicator (see Figure 5–2 (F) page 48 and Figure 5–4 page 50).

5.1.4 GafChromic® EBT films measurements.

Dose measurements of the irregular field shape, shown in Figure 5–2 (F) page 48, for electron beams of 6, 9, 12, 16 and 20 MeV for the Clinac 21-EX were carried out by GafChromic® EBT films (International Speciality Products, NJ, USA). Depth dose distributions were obtained by inserting GafChromic® films between two slabs of Solid Water® phantom (see Figure 5–3 (D) page 49). A water ultrasound transmission gel (Parker Laboratories, Inc. 286 Eldrige Road ; Fairfield, NJ 07004 ; USA) was used

to provide a tight fit of the film in the insert and as well to minimize the number of air bubbles between the film and Solid Water® surface.

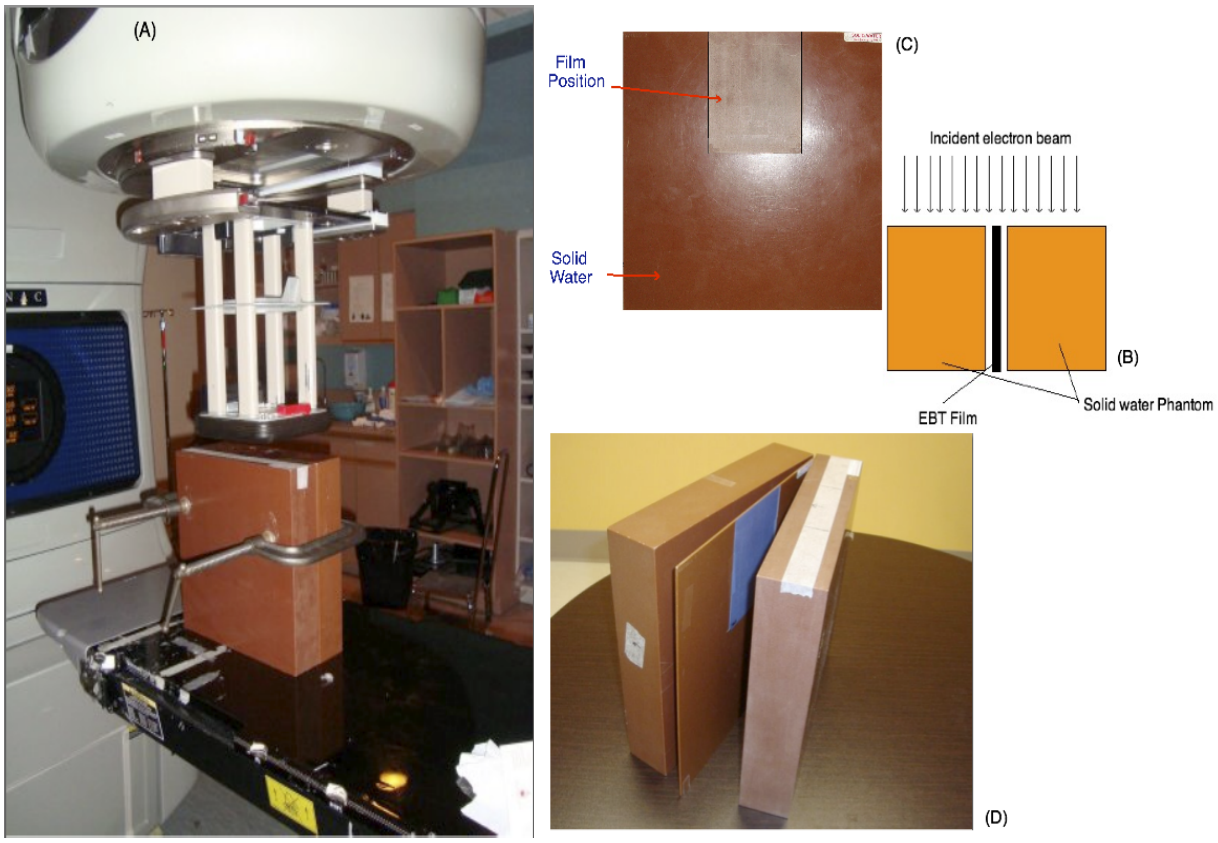

FIGURE 5–3 – *Depth dose setup measurements with film and Solid Water® phantom for irregular field.*
(A) *experimental set-up on the Varian linac 21-EX ;*
(B) *cartoon of the slice of the Solid Water® phantom exposed to electron beam ;*
(C) *homemade Solid Water® phantom used for irregular field measurements ;*
(D) *GafChromic® films & Solid Water® phantom combination set-up.*

The films were placed parallel to the electron beam central axis, as shown in Figure 5–3 (A) & (B) page 49, and aligned to the surface of the Solid Water® phantom. A special home-made Solid Water® phantom (see Figure 5–3 (C) & (D) page 49) was used to hold the films during the experiment. The films were placed between two slabs of Solid Water®. At least 10 cm of Solid Water® phantom was used on each side of the field. To minimize the number of air bubbles between the film

and the Solid Water® phantom, the overall Solid Water® assembly was also compressed with clamps (Figure 5–3 (A) page 49). The percentage depth dose measurements were performed at two predefined positions (PDD1 & PDD2) as specified in Figure 5–4 page 50. Finally, for the measurements of the lateral profiles, the films were placed in the solid phantom, perpendicular to the central axis at the respective depth of maximum dose $Z_{\max}$.

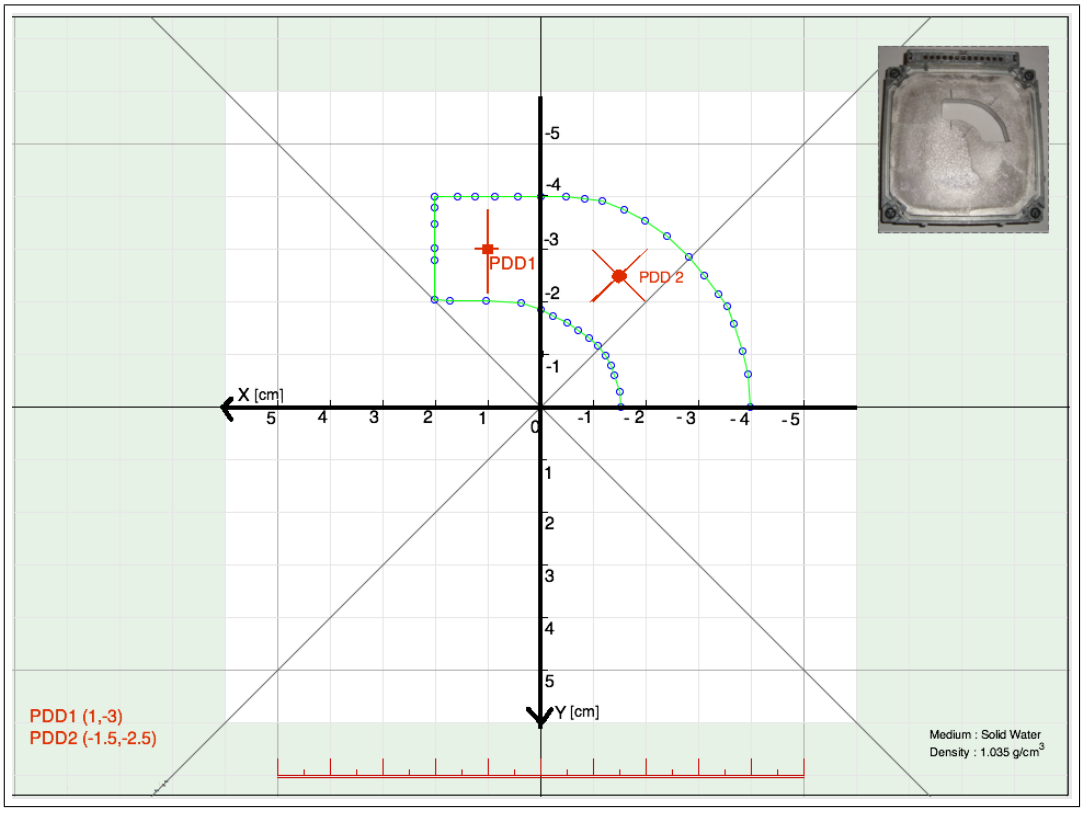

FIGURE 5–4 – *Position of measured percentage depth dose for the irregular cutout in place in the 10×10 cm² applicator size.*

5.1.5 Films calibration and post analysis.

Before GafChromic® EBT films were exposed to radiation, a pre-scan was performed with an EPSON® Expression 10000XL flatbed document scanner (Epson Seiko corporation, Nagano, Japan) for every film. Each EBT were scanned 3 times in transmission mode, at 150 dpi with all corrections turned off. One unexposed film

was also scanned so that background OD ($OD_{\text{background}}$) could be monitored and corrected for. After waiting at least 12 hours for self development, the GafChromic® EBT films were scanned again with the same scanner (see Figure 5–5 (A) page 51) and the corresponding pixel value was recorded. A home made MATLAB routine was used to extract the red component of the image, to smooth the data with a Wiener filter, to co-registrer, and to re-bin the data (see Figure 5–5 (B) page 51).

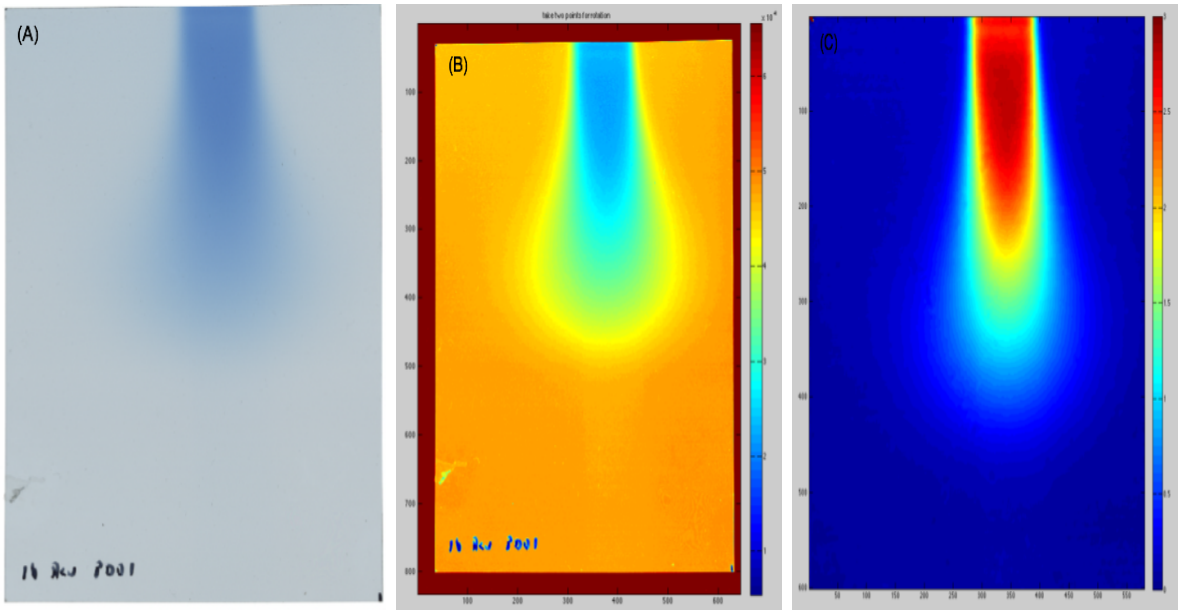

FIGURE 5–5 – *EBT GafChromic® films :*
(A) *exposed to radiation of a 16 MeV electron beam ;*
(B) *red component of the exposed film ;*
(C) *dose distribution.*

Net optical density ($netOD$) matrices were then calculated, following Devic *et al* [4–7], as:

$$netOD = OD_{\text{film}} - OD_{\text{background}} = \log\left(\frac{I_{\text{unexposed}} - I_{\text{background}}}{I_{\text{exposed}} - I_{\text{background}}}\right) \tag{5.1}$$

where $I_{\text{unexposed}}$, $I_{\text{background}}$, and I_{exposed} are the pixel values in the red component of the unexposed, background, and exposed images. Finally, conversion to dose (see Figure 5–5 (C) page 51) was performed using a fitted relation between dose and net

optical density (see Figure 5–6 page 52):

$$\text{Dose} = 5.183613456 \times netOD + 13.79982767 \times netOD^{2.5} \qquad \text{[Gy]} \qquad (5.2)$$

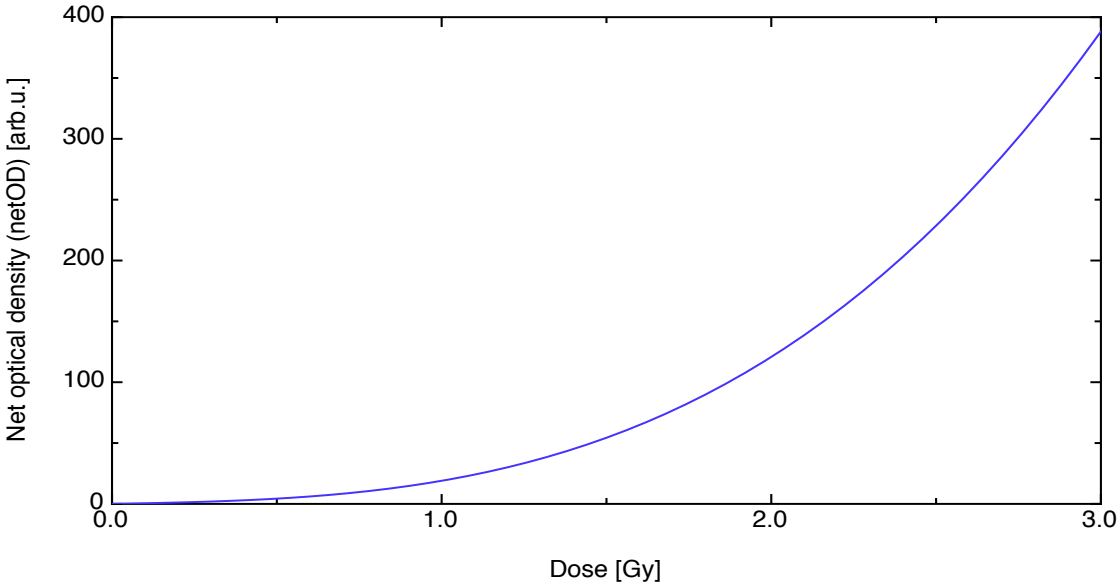

FIGURE 5–6 – *Film calibration curve for EBT GafChromic® film for the batch.*

Dose matrices were saved in TIFF (Tagged Image File Format) image file format.

5.1.6 Measurements setup.

Measurements of the central axis percentage depth dose curves and transverse beam profiles at depth of maximum dose were performed with a specific setup. This setup is summarized in Table 5–4 page 53.

TABLE 5–4 – *Acquisition parameters for measurements of PDDs and profiles.*

Parameters	Values
Phantom Material 1	Liquid Water
Phantom Material 2	GafChromic® films
Phantom size	(40×40×40) cm^3
Film size	(12×12) cm^2
Source to Surface Distance (SSD)	100 cm
Air Temperature	22.1^0C
Air Pressure	747.8 mmHg
Relative Humidity	50 %
Field size at Phantom Surface	see Table 5–3 page 47
Polarizing Voltage	300 Volt
Positioning Accuracy	0.05 mm
Reference Point of the IC-10 chamber	On the Central axis at the center of the cavity volume

5.2 Monte Carlo Model.

The construction of an electron beam model using Monte Carlo techniques is more challenging as compared to conventional planning system such as Eclipse or CadPlan (Varian Medical Systems, Inc., Palo Alto, CA 94304). Indeed, the commissioning procedure requires accurate clinical beam data and extensive information about the treatment head geometry. Precise knowledge of each and every component of the head is required in order to correctly calculate the dose deposition. The initial step to model the VARIAN Clinac 21-EX treatment head using EGSnrc-BEAMnrc MC codes [8] starts with the construction of the major components of the linac.

5.2.1 Monte Carlo BEAMnrc model of the VARIAN Clinac 21-EX.

A discussed in Chapter 4, in BEAMnrc code, the accelerator head is constructed from the definition of a series of component modules (CM), each of which takes part in the simulation of the head. The dimensions, composition, and location of each CM is obtained using the manufacturer informations. However, as we will discuss later, these informations are not necessarily accurate. Therefore, physical measurements are generally required. Each CM is defined to occupy a precise location in the space

perpendicular to the beam's central axis. Using this design, the linear accelerator is built by stacking of top of each other the different component modules. For our work, BEAMnrc was used to model a Varian Clinac 21-EX linear accelerator.

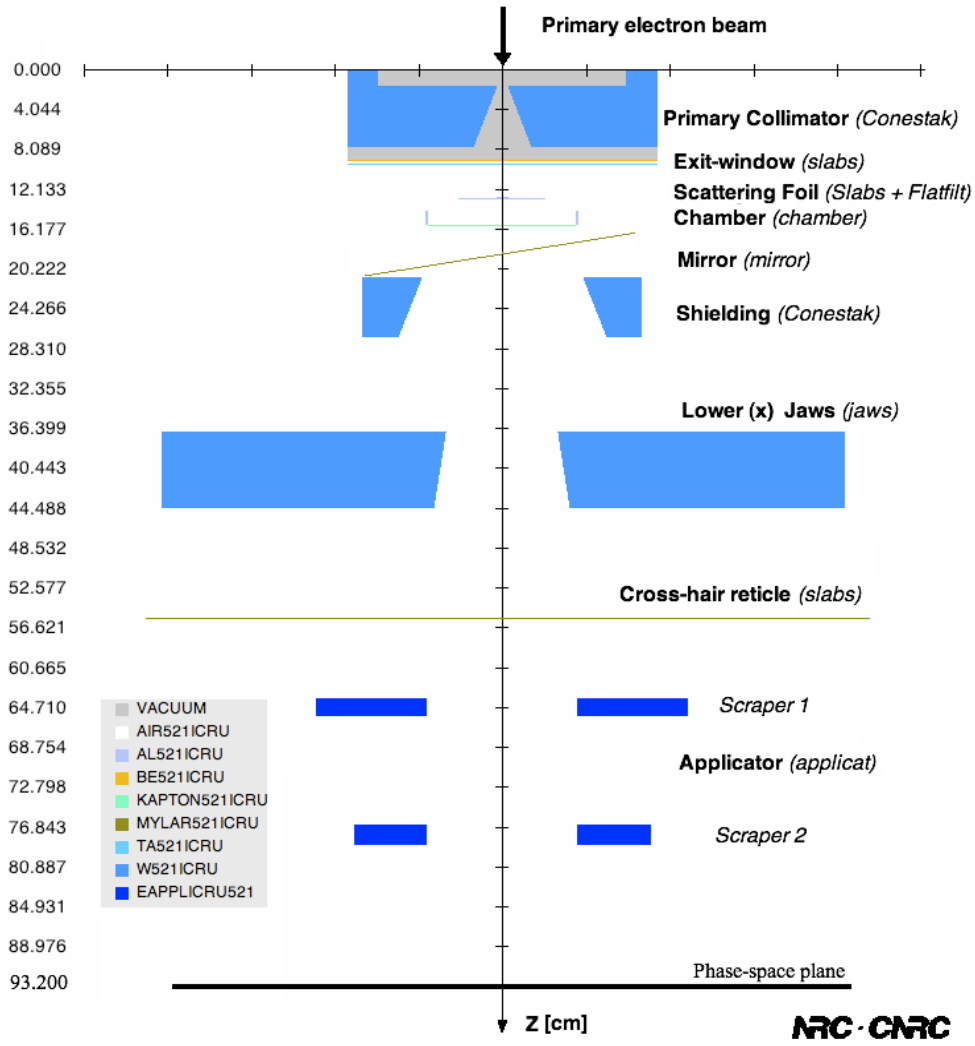

FIGURE 5–7 – *Schematic overview of the Varian Clinac 21-EX treatment head modeled using the BEAMnrc graphical user interface. The distances in Z-direction correspond to the distances from the corresponding BEAM component module (CM) to the reference plane. In parenthesis are given the BEAM CMs used to construct our model.*

The exit window, the primary collimator, the scattering foil, the monitor ion chamber, the shielding, the upper and lower jaws, the mirror, the cross-hair and the

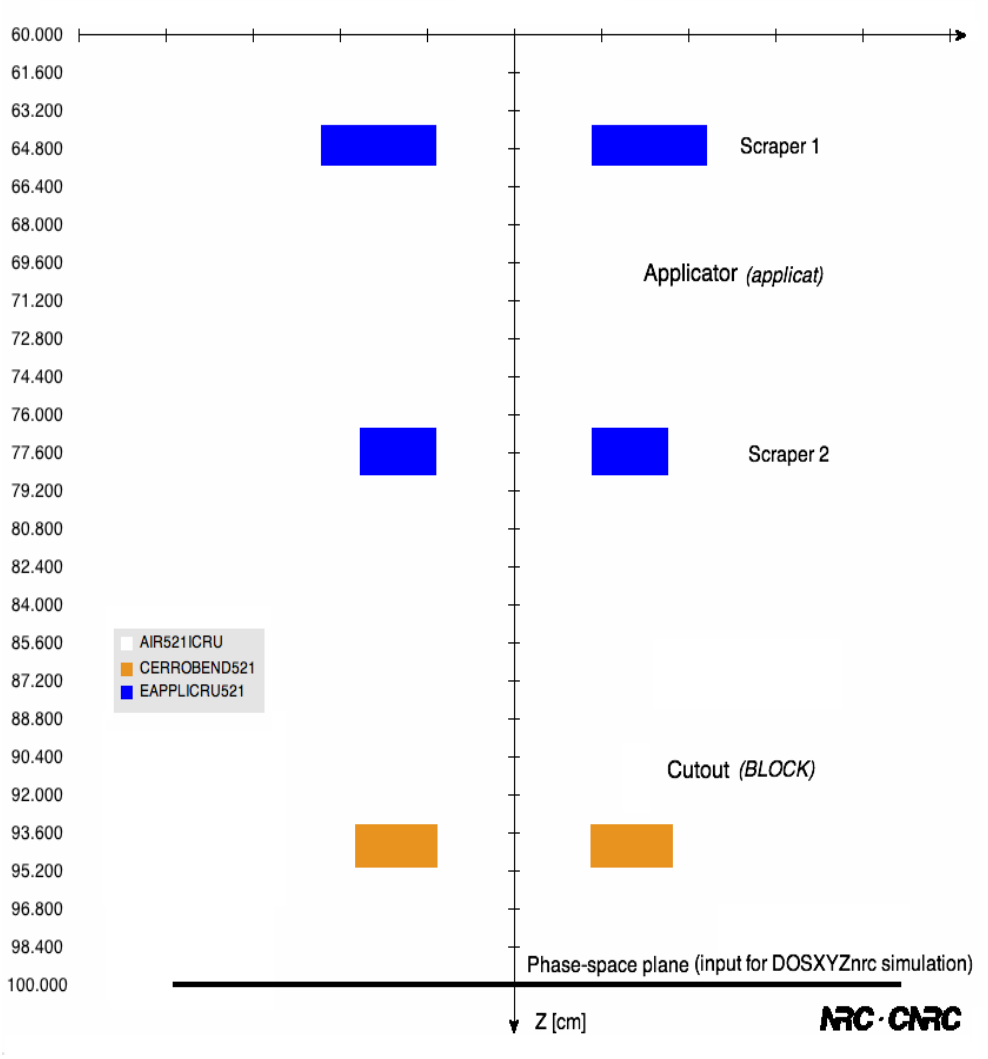

FIGURE 5–8 – *Schematic overview of the Varian Clinac 21-EX (10×10) cm² applicator along with a (10×10) cm² cutout modeled with the BLOCK component module of the BEAMnrc graphical user interface. The distances in Z-direction corresponds to the distance from the corresponding BEAM component module (CM) to the reference plane. In parenthesis are given the BEAM CMs used to construct our model.*

applicators along with their scrapers were defined as CMs according to the information provided by Varian [9]. Figure 5–7 page 54 shows a schematic representation of our MC model, made of several CMs, of the Varian Clinac 21-EX. Mono energetic electrons are set in motion at the level of the vacuum window. Theses electrons are

then transported throughout the treatment head and a phase-space file [1] is recorded from the particle information just above the last scrapper where the cutout is inserted. Each cutout was modeled with the CM BLOCK (see Figure 5–8 page 55) and inserted at 93.20 cm away from the exit window. This way, the model allows us to simulate square, rectangular and circular fields. However, the BLOCK component module does not allow the simulation of concave cutouts. Therefore, for irregular fields, a previously developed EGSnrc code [10] have been used (CutoutManager [11] - see Figure 5–9 page 56). This EGSnrc user code transports particles of the phase-space file generated above the cutout through any irregular custom cutout. The last step is to use the phase-space file created below the cutout as input to DOSXYZnrc for further simulation into a CT patient.

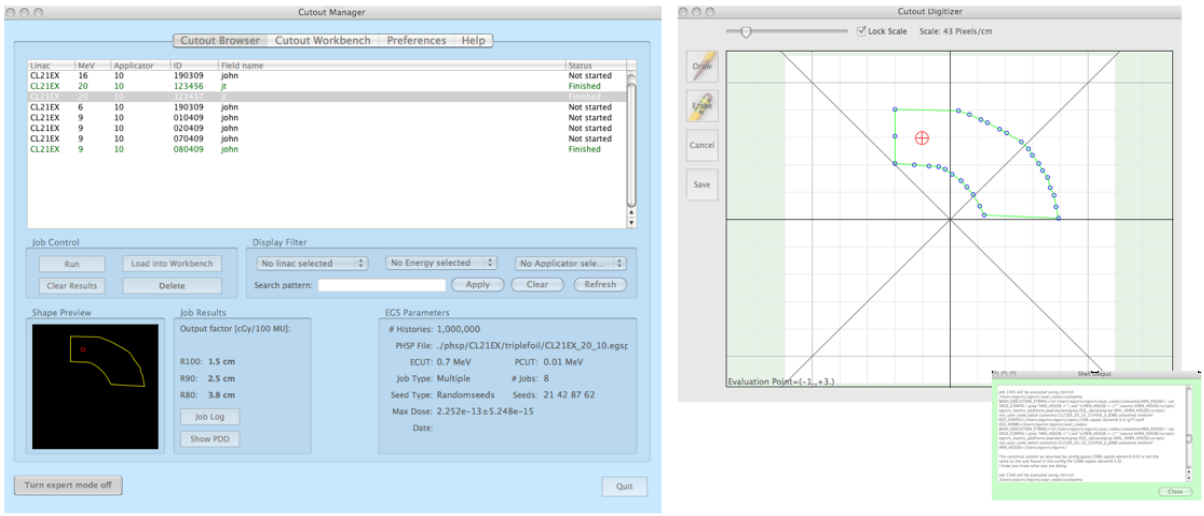

FIGURE 5–9 – *Snapshot of the CutoutManager [11]. An application used to simulate the transport of particles through a specific custum-made cutout.*

1. The transport of particles through the linac treatment head outputs a phase-space file that will record the history of every simulated particles, i.e. the energy of the particle, the charge of the particle, where the particle has been, if the particle is a secondary particle, fluences, etc

5.2.2 Electron beam source type.

As explained previously, treatment head simulation begins with accurate informations of the different components of the linac using manufacturer specifications. However actual accurate information of the incident electron beam energy and distributions are not yet available. Possible sources include isotropic point source with mono-directional fluences, circular beam with a 2D Gaussian distribution, isotropic cylindrical source, etc. Extensive work has been done to obtain the most accurate specifications for the electron beam source since the accuracy of the dose calculations will highly depend on it. Therefore, in this work, various fine-tuning of the incident electron source geometry along with the energy spectrum has been built and tested by comparing the calculated dose in water phantom against measured data. An isotropic point source ($ISOURC = 1$) with a circular beam of radius 0.04 cm ($RBEAM$) located 5.5 cm above the first BEAMnrc component module ($DISTZ$) was found to yield the best agreement between measured and calculated data (see Figure 5–10 page 57).

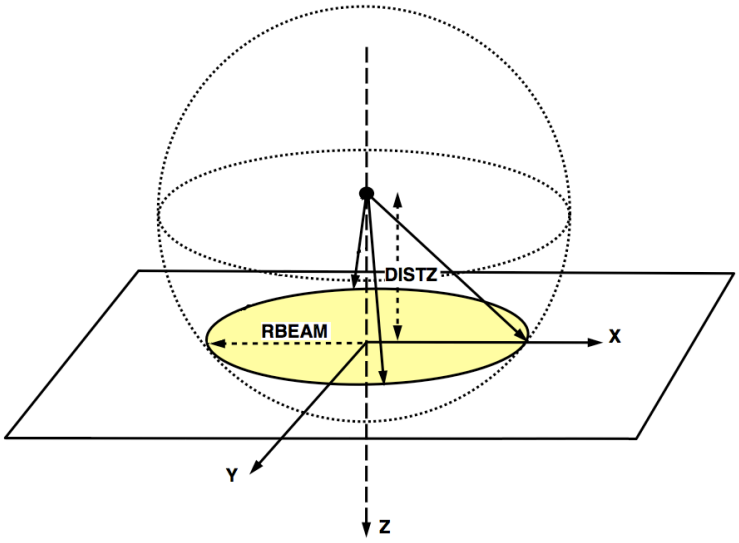

FIGURE 5–10 – *Simulated source type for electron beam - ISOURC=1: isotropic point source on Z-axis [12].*

The next step was then to determine the electron beam energy at the exit window. A first estimate was derived using the depth of 50% in water (R_{50}) from the measured percentage depth dose curves. As outlined by the ICRU report 21 [13], the energy of the electron beam at the water surface can be estimated using Equation 3.3 page 30. A second guess of the primary electron energy was obtained by comparing the calculated dose distribution (PDD and profiles) with measurement. The simulation was then repeated and reiterated until the percentage difference between the measured and calculated R_{50} was within 2%. Table 5–5 page 58 tabulates the tuned electron beam energy used for our model.

TABLE 5–5 – *Monoenergetic incident electron beam energies found to model our clinical beams.*

Nominal Energy [MeV]	6 MeV	9 MeV	12 MeV	16 MeV	20MeV
MC incident Beam energy [MeV]	6.7 MeV	9.7 MeV	13.3 MeV	17.7 MeV	22 MeV

5.2.3 Scattering foil parameters.

The component of the linac head that has the largest impact on the MC simulations is the scattering foil assembly. It is therefore crucial to accurately model this component since the accuracy of the calculations will depend on it. As we explained previously, a treatment head simulation begins with accurate knowledge of the different components of the linac head using the manufacturer specifications. Varian [9] claims the scattering foil to be composed of an upper and lower part with dimension and design as specified in Table 5–6 and Table 5–7 page 59. The primary and secondary foils are concentric disks made of tantalum with dimensions that vary as a function of beam energy.

TABLE 5–6 – *Dimension of the upper scattering foil of type III [9] as stated by Varian*

Corresponding Energy	Layer Thickness [cm]
6 MeV:	0.005080
9 MeV:	0.005080
12 MeV:	0.007620
15 MeV:	0.013208
16 MeV:	0.016510
18 MeV:	0.019558
20 MeV:	0.022860
22 MeV:	0.022860

TABLE 5–7 – *Dimension of the lower scattering foil of type III [9] as stated by Varian.*

Electron Beam Energy	Concentric Disc Nb	Layer Thickness [cm]	Disk Diameter [cm]
6, 9 MeV:	Disk 1	0.02286	0.80010
	Stand 1	0.00762	5.61706
	Disk 2	0.10160	0.99822
	Stand 2	0.00762	5.61706
12 MeV:	Disk 1	0.04826	0.80010
	Stand 1	0.00762	5.61706
	Disk 2	0.10160	0.99822
	Stand 2	0.00762	5.61706
15, 16, 18 MeV:	Disk 1	0.05080	0.39878
	Disk 2	0.05080	0.59944
	Disk 3	0.05080	0.80010
	Disk 4	0.05080	0.99822
	Stand	0.01524	5.61706
20, 22 MeV:	Disk 1	0.10160	0.59944
	Disk 2	0.05080	0.80010
	Disk 3	0.05080	0.99822
	Stand	0.01524	5.61706

According to Varian's specifications, the concentric disks for the lower scattering foil are supported by a 0.006 inch (0.01524 cm) aluminum plate for all electron beam energies (Figure 5–11 page 60). However this information is incorrect. Previous research [14] has shown that the geometry of the upper and lower scattering foil for 6, 9 and 12 MeV differs form the current manufacturer specifications. Direct measurements of the foils revealed additional stands sandwiched between the stacking

foils. This approach has been used for our model to simulate the 6, 9 and 12 MeV scattering foils and Figure 5–12 page 60 illustrates our geometry.

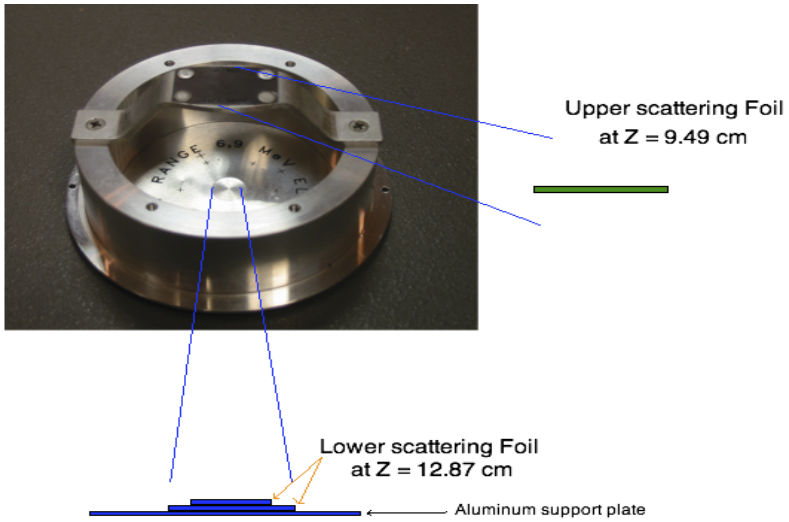

FIGURE 5–11 – *BEAMnrc model of the Varian Clinac 21-EX scattering foils for the 16 & 20 MeV. Varian [9]*

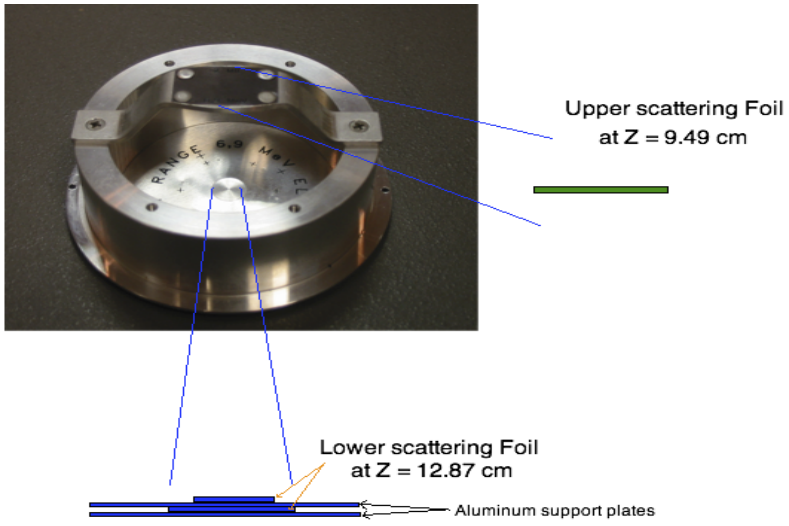

FIGURE 5–12 – *BEAMnrc model of the Varian Clinac 21-EX scattering foils for the 6, 9 & 12 MeV. Varian [9]*

5.2.4 Monte Carlo simulation time.

As mentioned in the previous Chapter, the major drawback of the Monte Carlo method is the computing time required to obtain an acceptable statistical uncertainty in the simulated quantities. The definition of Monte Carlo computation efficiency ϵ for large number of histories is given by [15]:

$$\epsilon = \frac{1}{T.s^2} \tag{5.3}$$

Where T is the computing time required to obtain the variance s^2. Therefore, an increase by 100 of the computing time is required in order to decrease the statistical uncertainty by 10 (for constant efficiency). It has been shown [16] that in order to achieve a 1% statistical uncertainty in the dose distribution in a water phantom made of 1 cm^3 cubic voxels, about 10^4 simulated electrons were needed for every 1 cm^2 area within the field. The number of particles per unit area would increase for smaller voxels to achieve the same statistical uncertainty. For our model, a particle density of 100 000 particles/cm^2 were used to achieve a 0.1% statistical uncertainty in the dose distribution in a water phantom of (0.5×0.5×0.5) cm^3 cubic voxels. This means that between (60×10^6) to (800×10^6) number of independent events (or histories [2]) were simulated in the accelerator head in order to achieve this 0.1% statistical uncertainty. The linac treatment head simulation and the dose calculation within the experimental phantoms were performed on a computer cluster at the Montreal General Hospital and at the Jewish General Hospital. This cluster is made of 6 machines all interconnected together by a network:

– 2 distinct Mac Pro computers Intel Xeon 4 cores 2.6 GHz CPU

2. the number of histories increases with decreasing incident electron energy for fixed field size and decreases with decreasing field size for fixed electron beam energy.

- 2 distinct Mac Pro computers Intel Xeon 8 cores 3.2 GHz CPU
- 1 sub-cluster name "blade" made of 8 distinct Intel dual cores of 1.2 GHz.

The overall cluster consists of 40 processing cores. This approach offers a convenient way to use multiple processors to perform the calculation. Different batches of simulation are executing independently and at the end of each simulation the multiple outputs are combined together. The final result is identical, within statistical uncertainties, to the one that would have been obtained on a single processor. This approach offers a significant time saving for the simulation and allows one to obtain better statistics in a shorter overall calculation time (better efficiency). The total CPU time required to simulate five nominal electron energies (6, 9, 12, 16 & 20 MeV) and six cutouts was close to 336 hours (2 weeks). Because of the iterative process of fine-tuning electron incident energy and other accelerator parameters, the overall CPU time for commissioning all the beams properly was about two months.

5.2.5 MMCTP - EGS/BEAMnrc parameters.

One of the goals of our project was to incorporate our electron beam model into an in-house treatment planning system. This was successfully accomplished through a research radiotherapy environment for Monte Carlo treatment planning: the McGill Monte Carlo treatment planning - **MMCTP** [17]. The application consists of a graphical user interface (GUI) (see Figure 5–13 page 63), and provides a flexible software environment to integrate various modalities such as our electron beam model. MMCTP has all the informations, and necessary tools to read EGSnrc/BEAMnrc input files and it is a very powerful research platform which incorporates many functionalities. One of the available option is the specification of the number of BEAMnrc particle per cm^2 deposited in the phase-space. Generally, the number of histories *NCASE* in BEAMnrc is requested for the simulation, and a certain particle density

is reached on the phase-space. Whereas in MMCTP the desired particle density is requested and an history number is given for the siumlation. The history number is calculated thought the simulation of a test run containing few histories, between 1000 and 2000 in our case. As mentioned previously, in order to minimize the computing time and statistical errors, a particle density of 100 000 particles/cm^2 were used, corresponding in average [3] to the transport of $\left((60 - 800) \times 10^6\right)$ primary electrons. The other BEAMnrc parameters were consistent and conservatively chosen to reduce calculation time (see Table 5–8 page 64). The electron creation and the minimum energy cutoff, *AE* and *ECUT*, were both set to 0.7 MeV as the total energy. Information about these parameters can be found in the EGSnrc manual [18].

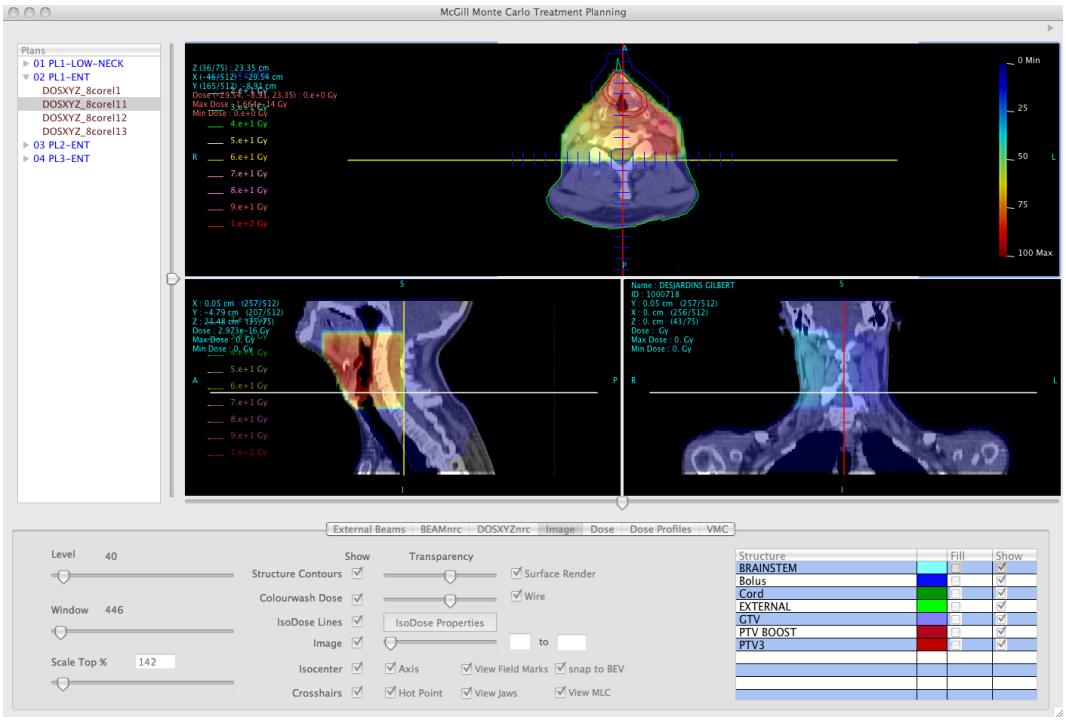

FIGURE 5–13 – *Snapshot of the McGill Monte Carlo treatment planning MMCTP [17].*

3. for all clinical energy 6, 9, 12, 16 & 20 MeV and for all applicators & cutouts sizes and shapes.

After obtaining an adequate model of the linac treatment head, phase-space file were recorded just before the last scraper where the cutout is insert. This phase-space file was then used to simulate the transport of particles throughout any cutout shapes, using the CutoutManager [10, 11] application. The resulting phase-space file can later be used as an input for dose calculation in a water phantom or in a CT patient using the DOSXYZnrc calculation code, last step of our simulation.

TABLE 5–8 – *EGSnrc transport parameters in BEAMnrc used for our simulations of the Varian Clinac 21-EX treatment head.*

Parameter	Value	Parameter	Value
Incident Particle	electron	Electron step Algorithm	PRESTA-II
Medium	AIR521ICRU	Spin effects	ON
ECUT	0.7 MeV	Electron Impact Ionization	Off
PCUT	0.01 MeV	Brems angular sampling	Simple
Photon Forcing	Off	Breams Cross sections	BH
Electron Range rejection	Off	Bound Compton scattering	Off
Source Number	ISOURC = 1	Pair angular sampling	simple
Xlmax	0.5	Photoelectron angular sampling	Off
BCA	EXACT	Rayleigh scattering	Off
Atomic relaxations	Off	Photon cross-sections	Storm-Israel
ESTEPE	0.25	ESAVEGlobal	0 MeV
SMAX	10^{10} cm	Skin depth for BCA	0 cm

5.2.6 Depth-dose calculations using DOSXZnrc.

Finally, dose calculation in a voxel geometry mimicking a water phantom was performed using the Monte Carlo code DOXYZnrc. The accuracy of the simulation is improved with the incorporation in DOSXYZnrc of the spin effect, known to affect the calculation of the 50% dose depth (R_{50}). Table 5–9 page 65 enumerates the EGSnrc transport parameters chosen for the DOSXYZnrc calculations in water phantom.

TABLE 5–9 – *EGSnrc transport parameters in DOSXYZnrc used for the simulation dose deposition in water phantom and in Solid Water® phantom.*

Parameter	Value	Parameter	Value
ECUT	0.521 MeV	Electron Impact Ionization	Off
PCUT	0.01 MeV	Spin effects	ON
IWATCH Output	none	Electron step Algorithm	PRESTA-II
ESTEPE	0.25	Brems angular sampling	Simple
SMAX	5 cm	Breams Cross sections	BH
Xlmax	0.5	Bound Compton scattering	Off
Photon splitting number	1	Pair angular sampling	Simple
BCA	EXACT	Photoelectron angular sampling	Off
HOWFARLESS	On	Rayleigh scattering	Off
Range rejection	Off	Atomic relaxations	Off
Skin depth for BCA	0 cm	Photon cross-sections	Storm-Israel

References

[1] IAEA. Absorbed dose determination in external beam radiotherapy - an international code of practice for dosimetry based on standards of absorbed dose to water. Technical Report Technical report Series No. 398, IAEA - International Atomic Energy Agency., 2000. Sponsored by the IAEA, WHO, PAHO and ESTRO.

[2] IBA. IBA bleu water phantom - http ://www.iba-dosimetry.com/.

[3] Varian Medical System Web-Page. http ://www.varian.com/.

[4] Slobodan Devic, Jan Seuntjens, Gyorgy Hegyi, and Ervin B. Podgorsak. Dosimetric properties of improved gafchromic™ films for seven different digitizers. *Med. Phys.*, 31, September 2004.

[5] Slobodan Devic, Jan Seuntjens, Edwin Sham, and Ervin B. Podgorsak. Precise radiochromic™ film dosimetry using a flat-bed document scanner. *Med. Phys.*, 32, July 2005.

[6] Slobodan Devic, Nada Tomic, Zhiyu Pang, Jan Seuntjens, and Ervin B. Podgorsak. Absorption spectroscopy of EBT model GAFCHROMIC™ film. *Med. Phys.*, 34, January 2007.

[7] Slobodan Devic, Nada Tomic, Christopher G. Soared, and Ervin B. Podgorsak. Optimizing the dynamic range extension of a radiochromic™ film dosimetry system. *Med. Phys.*, 36, February 2009.

[8] Kawrakov I and Rogers D W O. EGSnrc / BEAMnrc / DOSXYZnrc. EGS electron gamma source. Pirs, NRCC - Canada Ottawa - National Research Council., 2003.

[9] Montreal General Hospital. Varian oncology systems, Monte Carlo project. Information Serial Number 60A, Varian, 2004.

[10] Claude Albaret. Automated system for Monte Carlo determination of cutout factors of arbitrary shaped electron beams and experimental verification of Monte Carlo calculated dose distribution. Master's thesis, McGill University, Montreal General Hospital 1650 avenue cedar Montreal, Quebec H3G 1A4, 2004.

[11] Jurgen Last. Cutout Manager - A stand-alone software system to calculate output factors for arbitrarily shaped inserts with Monte Carlo technique.

Master's thesis, McGill University, Montreal General Hospital 1650 avenue cedar Montreal, Quebec H3G 1A4, 2008.

[12] Walters B, Kawrakow I, and Rogers D W O. DOSXYZnrc users manual. PIRS 794revB, NRCC, 2004.

[13] ICRU. Radiation dosimetry : Electrons with initial energies between 1 and 50 MeV. PIRS 21, ICRU - International Commission on Radiation Units and Measurements, 1972. Bethesda, Maryland.

[14] Genevieve Jarry. *Study of Novel Techniques for Verification Imaging and Patient Dose Reconstruction in External Beam Radiation Therapy.* PhD thesis, McGill University, Montreal General Hospital - 1650 avenue Cedar Montreal Quebec H3G 1A4, 2007.

[15] B R B Walters ; O. Kawrakow ; and D W O Rogers. History by history statistical estimators in the BEAM code system. *Med. Phys.*, 29 :2745, 2002.

[16] Rogers D W O Ma C-M, Faddegon B A and Mackie T R. Accurate characterization of monte carlo calculated electron beams for radiotherapy. *Phys. Med. Biol.*, 24 :401–16, 1997.

[17] Alexander A, DeBlois F, and Seuntjens J. MMCTP a radiotherapy research environment for Monte Carlo and patient-specific treatment planning. *Med. Phys.*, 33 :2293, 2006.

[18] Kawrakov I and Rogers D W O. The EGSnrc code system : Monte Carlo simulation of electron and photon transport. Pirs-701, NRCC - Canada Ottawa - National Research Council., 2003.

Chapitre 6
RESULTS AND DISCUSSION

Contents

Commissioning a MC model for a medical linear accelerator for electron beam starts with exhaustive measurements of relative dose within a phantom. A collection of PDD and dose profiles curves at selected depths has to be measured for many discrete field sizes (applicator sizes) at each electron beam energies. These measurements are then compared to the calculated dose distributions obtained using our Varian Clinac 21-EX model. These measurements were used to optimize our model, i.e. to adjust the Monte Carlo model and simulation parameters until a reasonable match between measured and calculated dose is reached. In this Chapter we are presenting the agreement between measured and calculated dose for the 6 - 20 MeV energy range for a selection of square, rectangular, circular and irregular cutouts.

6.1 Validation of the depth-dose curves reconstruction.

Figure 6–1 page 72 to Figure 6–4 page 75 (Plot (A) to (H)) show the comparison between measured and calculated percentage depth dose curves for an SSD of 100 cm, for five nominal energies (6, 9, 12, 16 & 20 MeV) and for six electron cutouts:

- (10×10) cm^2 applicator ; (10×10) cm^2 square cutout.
- (15×15) cm^2 applicator ; (15×15) cm^2 square cutout.
- (20×20) cm^2 applicator ; (20×20) cm^2 square cutout.
- (10×10) cm^2 applicator ; (3×8) cm^2 rectangular cutout.

– (10×10) cm^2 applicator ; circular cutout of 5 cm diameter.

– (10×10) cm^2 applicator ; irregular cutout.

All Monte Carlo calculated and measured curves were normalized to their maximum values. The statistical uncertainty for Monte Carlo dose calculations was kept smaller than 0.1%. Therefore, the error bars are smaller than the symbols and are not shown on the curves. Table 6–1 page 77 tabulates various depth dose parameters for the measured PDDs. In addition to the PDD curves, Table 6–2 page 78 to Table 6–4 page 80 summarize the agreements between measured and calculated key values. In these tables, calculated values of R_{100}, R_{90} and R_{50} are compared to measured values.

For most cases, the agreement is well within 2% for R_{50} and R_{90} but there are individual cases where the differences exceed 4%. However the agreement between measured and simulated values of R_{100} deviates by more than 2%, and it is even worst for measurements made with GafChromic® EBT films in Solid Water® phantom. One explanation for the important discrepancies observed could be due to some set-up errors during the commissioning of the irregular fields. One reason would be that air molecules could have penetrated the first few millimeters of the GafChromic® EBT films, or/and the films were not completely embedded in the Solid Water® phantom, and few millimeters were exposed to radiation in air. Recent work has shown as well that there is significant uncertainty in measuring build-up doses [1] and surface dose measurements are generally not easy tasks. These reasons might be the possible causes for the significant differences observed between measured and calculated R_{100}. Otherwise the dose distributions calculated after the depth of maximum dose and the calculated values of R_{50} and R_{90} agree well with the measured data (see Figure 6–3 (Plot F) page 74 & Figure 6–4 (Plot G) page 75). Moreover, as it has been mentioned in Chapter 3 section 3.1.2 page 27, only the dose from Z_{max} to the 90% dose level in the electron PDD should be used to cover the treatment target. The agreements of

our calculated data with the measured ones, after the depth of maximum dose, show that the performance of our model for small irregular field size is very acceptable.

Figure 6–2 plot (D) page 73 and Figure 6–3 plot (E) page 74 compare measured and calculated dose distribution for rectangular and circular fields. The data indicates that the agreement between the measured and the calculated values in the clinical range of depth dose distribution, i.e after the depth of maximum dose R_{100}, is within 2%, except for low energy electron beam of 6 MeV. Similar agreement is found for data taken with (10×10) cm^2, (15×15) cm^2 and (20×20) cm^2 applicators (Figures 6–1 page 72 & 6–2 page 73). The accuracy of our electron beam model in these configurations, is more than satisfactory.

Simulation of the depth dose curves for the irregular cutout at four different lateral positions for each energy were also performed (see Figure 6–5 plot (I) page 76). The results show that the effect of slightly shifting the position by few millimeters (2.5 mm and 5.0 mm) at which PDD has to be measured has a significant impact on the depth dose measurement curve by modulating the electron energy. This clearly demonstrates that measurements of cutout output factors are very sensitive to the point of measurement. This test confirms as well that the position of our measurements agrees with the calculations within 2.5 mm for 6, 9, 12 & 16 MeV electron beam energy i.e. measurement fits within the two misaligned positions tested: point P1 and point P2 of Figure 6–5 plot (J) page 76. Whereas for 20 MeV beam energy, the agreement between measured and calculated position is within 5.0 mm.

The capability of the model for calculating the relative dose for an open beam of (40×40) cm^2 size, without applicator mounted on the linac was also tested. Figure 5–4 plot (H) page 73 shows good agreement between measured and calculated dose in Solid Water® phantom. Discrepancies are nevertheless observed in the build region, certainly caused by a misalignment of the films with respect to the phantom,

as explained above.

6.2 Validation of the dose profiles reconstruction.

Having obtained this level of agreement for the standard field-size beams for central-axis depth dose, dose profile comparisons for the same field-size beams were examined. Figure 6–6 page 81 and Figure 6–7 page 82 illustrate profiles comparisons between calculations made with the MC model and measurements made with a cylindrical ionization chamber IC-10 for various clinical electron beam energy for:

- (10×10) cm^2 applicator ; (10×10) cm^2 square cutout.
- (15×15) cm^2 applicator ; (15×15) cm^2 square cutout.
- (10×10) cm^2 applicator ; (3×8) cm^2 rectangular cutout.
- (10×10) cm^2 applicator ; circular cutout of 5 cm diameter.

Excellent agreement is noted for all cases.

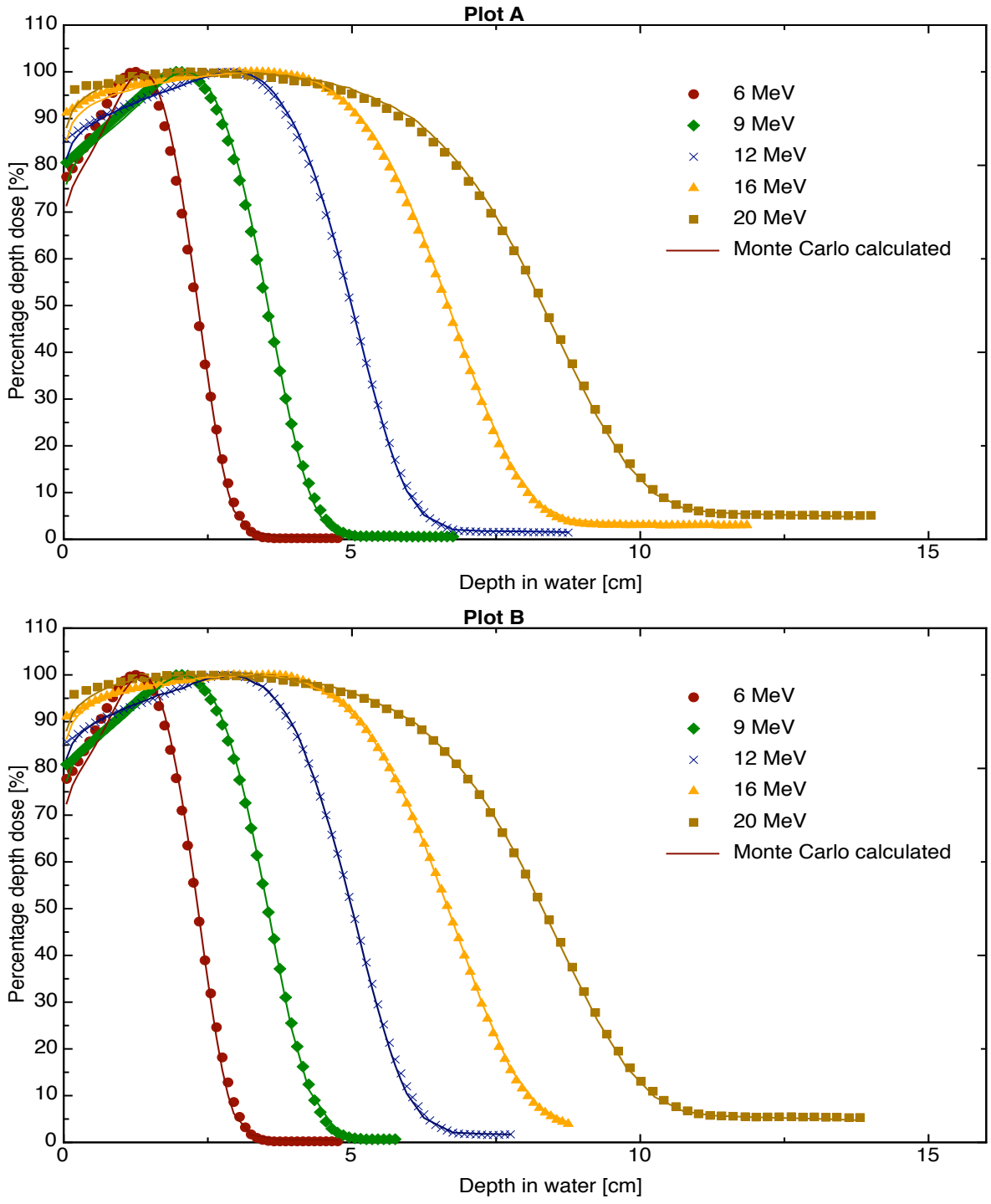

FIGURE 6–1 – *Percentage depth dose curves in water normalized at Z_{max} for 6, 9, 12, 16 & 20 MeV electron beam at 100 cm SSD calculated with Monte Carlo and measured with ionization chamber IC-10 for*:
Plot A: *(10×10) cm^2 applicator; (10×10) cm^2 square cutout.*
Plot B: *(15×15) cm^2 applicator; (15×15) cm^2 square cutout.*

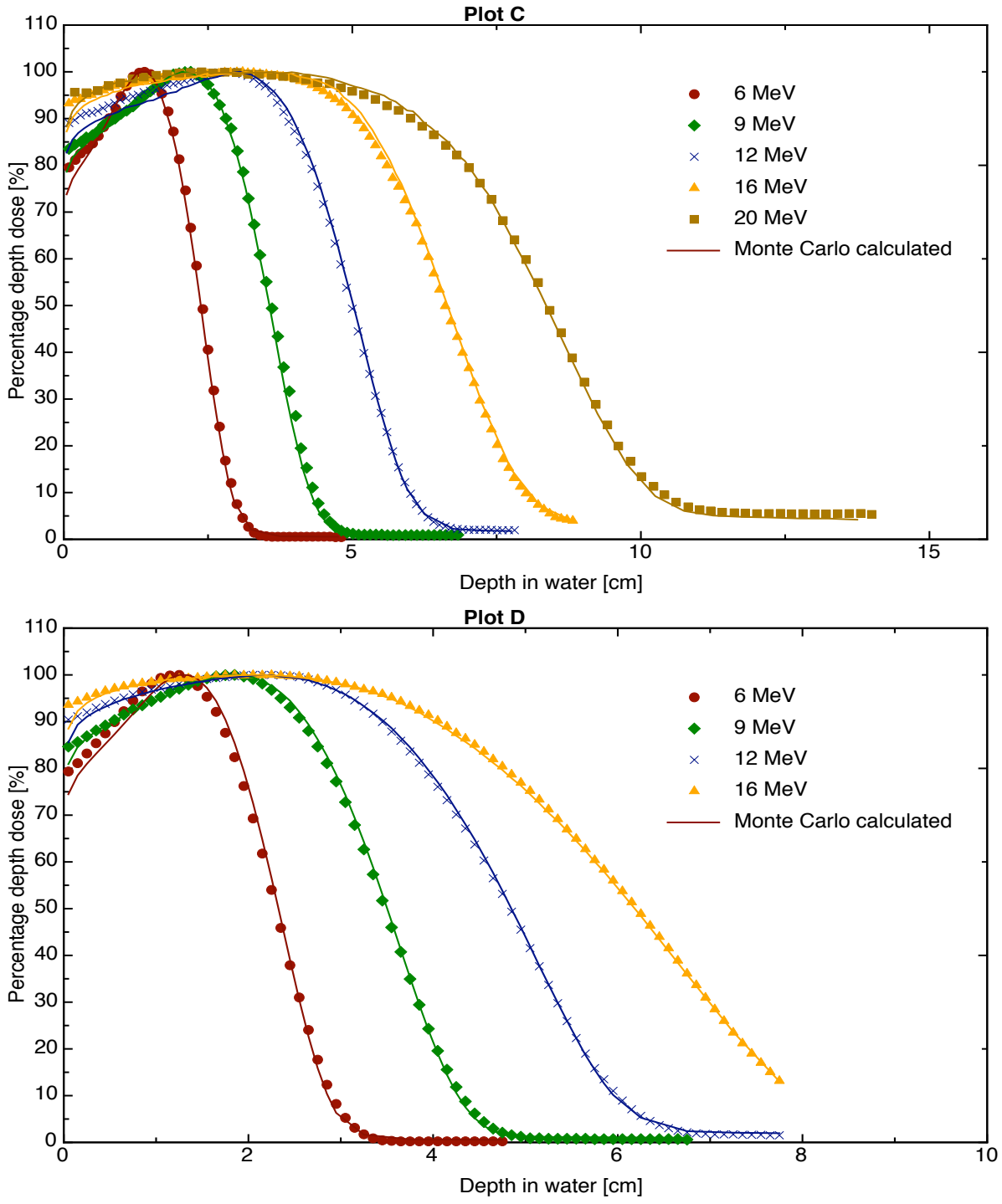

FIGURE 6–2 – *Percentage depth dose curves in water normalized at Z_{max} for 6, 9, 12, 16 & 20 MeV electron beam at 100 cm SSD calculated with Monte Carlo and measured with ionization chamber IC-10 for*:
Plot C: *(20×20) cm² applicator; (20×20) cm² square cutout.*
Plot D: *(10×10) cm² applicator; (3×8) cm² rectangular cutout.*

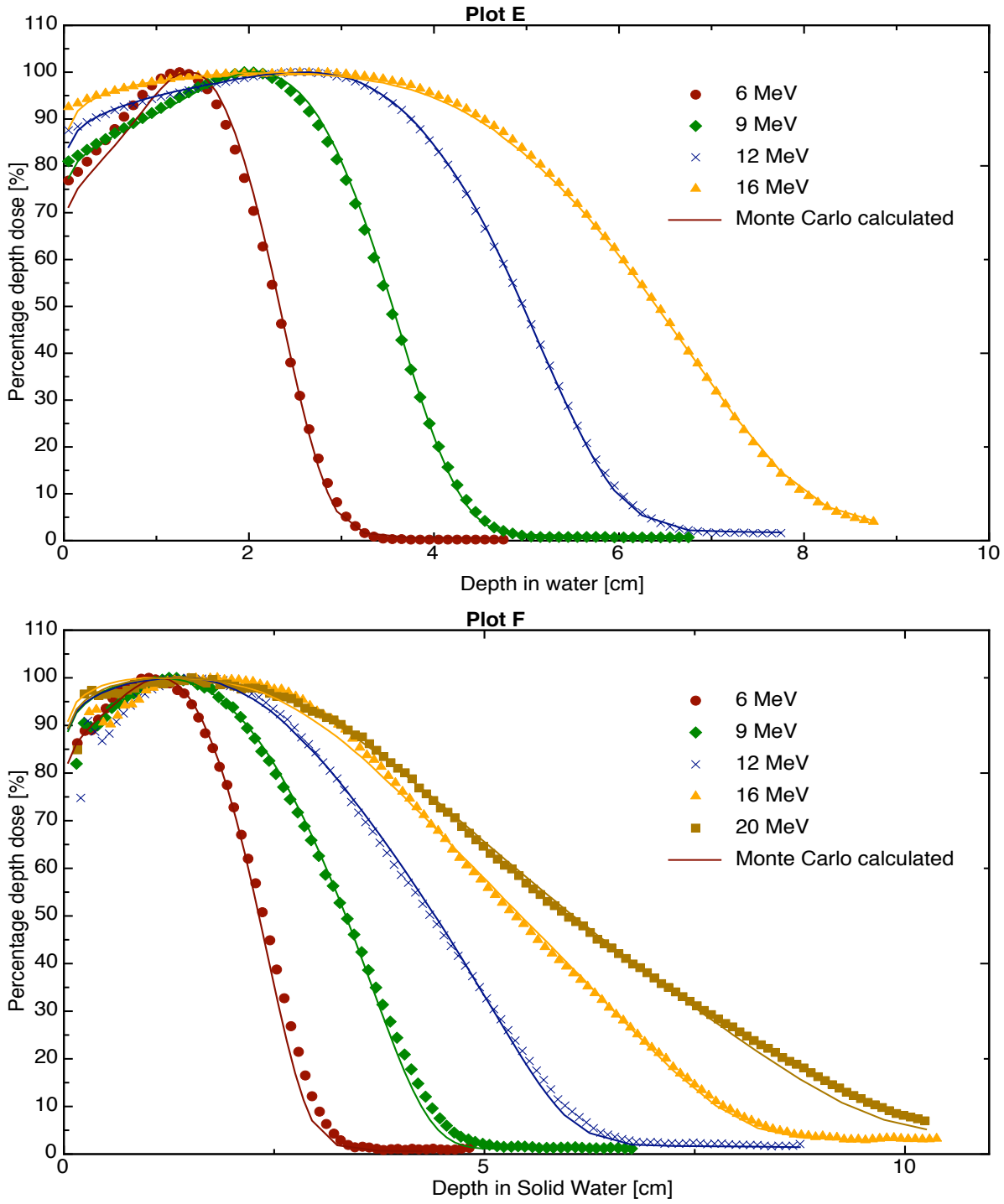

FIGURE 6–3 – *Percentage depth dose curves normalized at Z_{max} for 6, 9, 12, 16 & 20 MeV electron beam at 100 cm SSD*:
Plot E: *calculated with Monte Carlo in water and measured in water with ionization chamber IC-10 for (10×10) cm² applicator; circular cutout of 5 cm diameter.*
Plot F: *calculated with Monte Carlo in Solid Water® and measured in Solid Water® with GafChromic® EBT film for (10×10) cm² applicator; irregular cutout (position PDD1)*

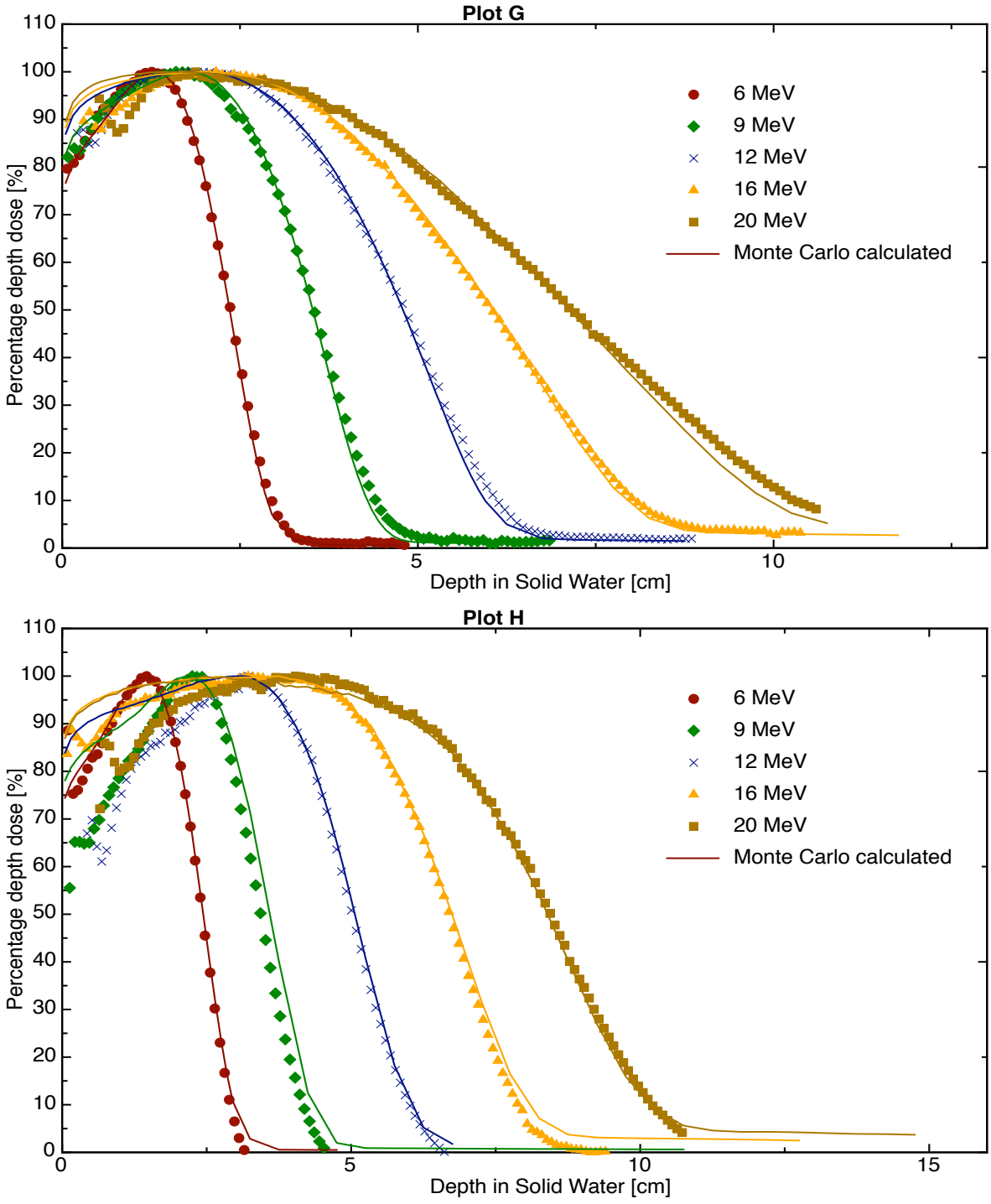

FIGURE 6–4 – *Percentage depth dose curves in Solid Water® normalized at Z_{max} for 6, 9, 12, 16 & 20 MeV electron beam at 100 cm SSD calculated with Monte Carlo and measured with*:
Plot G: *GafChromic® EBT film for (10×10) cm² applicator; irregular cutout (position PDD2)*
Plot H: *GafChromic® EBT film without applicator and cutout; field size (40×40) cm².*

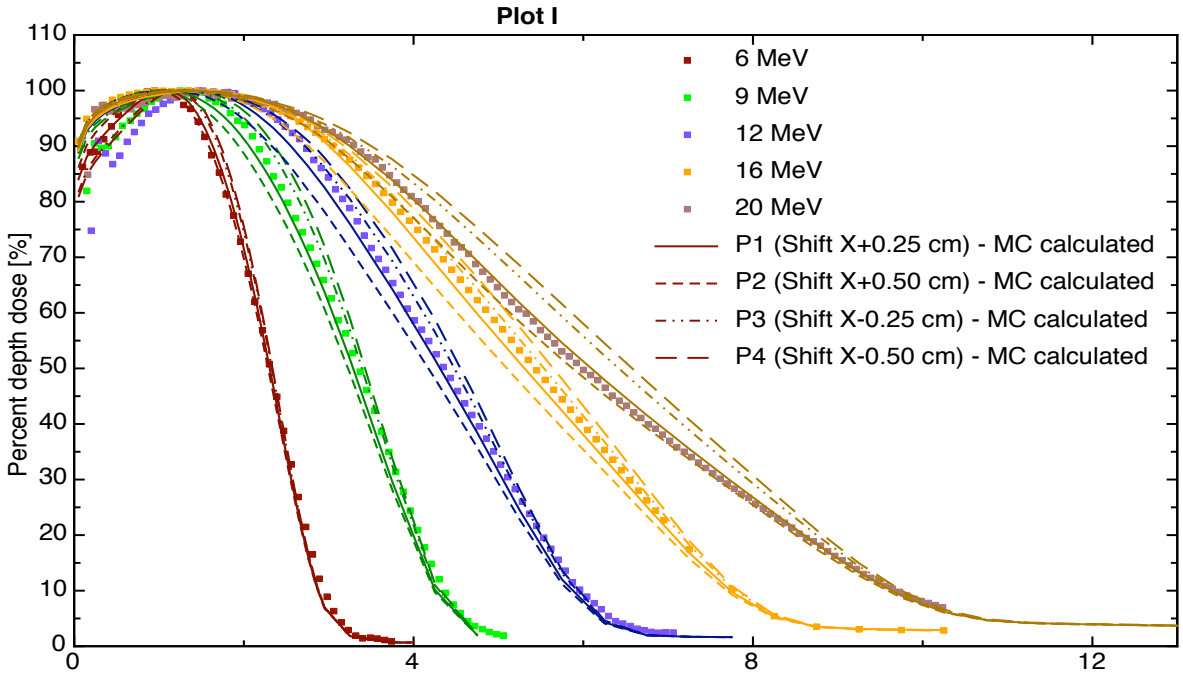

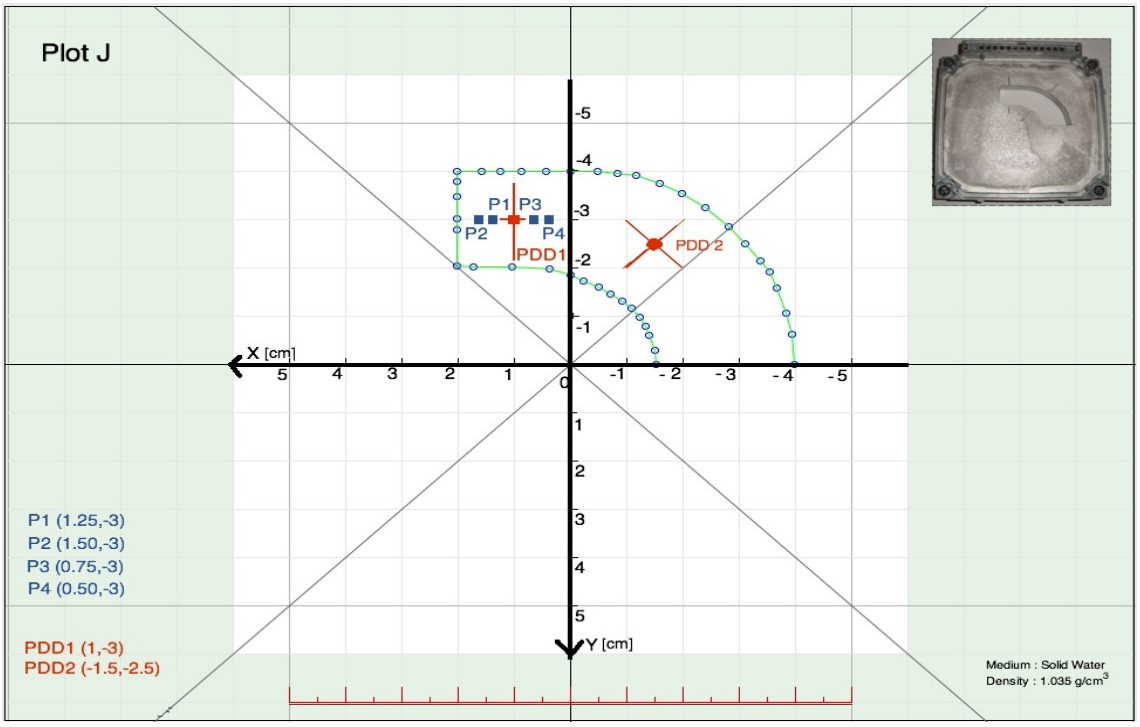

FIGURE 6–5 – ***Plot I***: *Percentage depth dose curves in Solid Water® normalized at Z_{max} for 6, 9, 12, 16 & 20 MeV electron beam at 100 cm SSD calculated with Monte Carlo for (10×10) cm² applicator ; irregular cutout.*
Plot J: *Position of measured percentage depth dose for the irregular cutout (PDD1 & PDD2), and the 4 different points of calculation P1(1.25,-3), P2(1.50,-3), P3(0.75,-3), P4(0.5,-3).*

TABLE 6–1 – *Depth dose parameters for electron beams*: ^{A}*measured with ionization chamber IC-10 &* ^{B}*measured with GafChromic® EBT films.*
Definitions: ^{C}***Brem Conta max***: *maximum bremsstrahlung contamination ;* ^{D}***Dose Grad G***: *Dose Gradiant G ;* ^{E}***Prob Energy*** $E_{\mathrm{p},0}$: *most probable energy* $E_{\mathrm{p},0}$

Cutout shape & applicator size	Beam Energy E_{nominal} [MeV]	Meas Depth $R_{\mathrm{p_{meas}}}$ [cm]	Meas Depth $R_{\mathrm{q_{meas}}}$ [cm]	^{C}Brem Conta *max* [%]	^{D}Dose Grad G	^{E}Prob Energy $E_{\mathrm{p},0}$ [MeV]	Mean Energy $\overline{E_0}$ [MeV]
	6 MeV^{A}	2.90	1.70	0.30	2.42	5.97	5.54
# Square cutout:	6 MeV^{B}	2.86	1.80	2.31	2.70	5.90	5.45
(10×10) cm^2	9 MeV^{A}	4.33	2.72	0.89	2.69	8.83	8.18
# Applicator:	12 MeV^{A}	6.00	3.93	2.48	2.89	12.20	11.60
(10×10) cm^2	16 MeV^{A}	7.93	5.29	3.87	3.00	16.07	15.49
	20 MeV^{A}	9.97	6.52	6.08	2.89	20.20	19.41
	6 MeV^{A}	2.92	1.72	0.26	2.43	6.02	5.38
# Square cutout:	9 MeV^{A}	4.33	2.77	0.76	2.78	8.83	8.25
(15×15) cm^2	12 MeV^{A}	6.02	3.94	2.32	2.89	12.24	11.65
# Applicator:	16 MeV^{A}	7.95	5.33	3.56	3.03	16.12	15.52
(15×15) cm^2	20 MeV^{A}	10.04	6.47	5.67	2.81	20.35	19.38
	6 MeV^{A}	2.92	1.89	0.61	2.83	6.02	5.60
# Square cutout:	9 MeV^{A}	4.37	3.08	1.18	3.39	8.91	8.36
(20×20) cm^2	12 MeV^{A}	5.94	3.98	2.29	3.03	12.07	11.60
# Applicator:	16 MeV^{A}	7.77	5.32	4.48	3.17	15.76	15.38
(20×20) cm^2	20 MeV^{A}	9.90	6.73	6.51	3.12	20.06	19.52
# Rectangular cutout:	6 MeV^{A}	2.91	1.69	0.35	2.37	6.01	5.36
(3×8) cm^2	9 MeV^{A}	4.34	2.63	1.13	2.54	8.86	8.11
# Applicator:	12 MeV^{A}	6.05	3.59	2.09	2.46	12.29	14.45
(10×10) cm^2	16 MeV^{A}	7.92	4.45	4.78	2.28	16.06	11.25
# Circular cutout:	6 MeV^{A}	2.90	1.70	0.55	2.42	5.99	5.36
Radius = 2.5 cm	9 MeV^{A}	4.32	2.75	1.08	2.74	8.83	8.20
# Applicator:	12 MeV^{A}	6.04	3.85	2.51	2.76	12.28	11.56
(10×10) cm^2	16 MeV^{A}	7.95	4.86	5.17	2.57	16.13	14.96
							
# Irregular cutout:	6 MeV^{B}	3.02	1.74	1.80	2.35	6.22	5.53
At PDD1	9 MeV^{B}	4.27	2.28	2.28	2.15	8.73	7.81
# Applicator:	12 MeV^{B}	5.78	2.56	4.38	1.79	11.74	10.16
(10×10) cm^2	16 MeV^{B}	6.93	3.26	5.70	1.89	14.06	12.53
							
# Irregular cutout:	6 MeV^{B}	2.92	1.80	1.47	2.61	6.04	5.51
At PDD2	9 MeV^{B}	4.36	2.71	2.84	2.63	8.90	8.25
# Applicator:	12 MeV^{B}	5.98	3.89	3.98	2.86	12.16	11.23
(10×10) cm^2	16 MeV^{B}	7.95	4.28	7.14	2.17	16.11	14.07

TABLE 6–2 – *Tabulated values for the measured and calculated depth of maximum dose R_{100}. Note:* $^{\boldsymbol{A}}$*data measured with ionization chamber IC-10in water phantom. &* $^{\boldsymbol{B}}$*data measured with EBT GafChromic® films in Solid Water® phantom.*

Cutout shape & applicator size	Beam Energy E_{nominal} [MeV]	Measured Depth R_{100} [cm]	Calculated Depth R_{100} [cm]	$\left\lvert \frac{R_{100}^{\text{Meas}} - R_{100}^{\text{Cal}}}{R_{100}^{\text{Meas}}} \right\rvert$
	6 MeV^A	1.40	1.35	3.57 %
# Square cutout:	6 MeV^B	1.37	1.35	1.85 %
(10×10) cm^2	9 MeV^A	2.10	2.15	2.38 %
# Applicator:	12 MeV^A	2.95	3.05	3.38 %
(10×10) cm^2	16 MeV^A	3.25	3.35	3.07 %
	20 MeV^A	2.20	2.55	15.90 %
	6 MeV^A	1.40	1.35	3.57 %
# Square cutout:	9 MeV^A	2.05	2.05	0.00 %
(15×15) cm^2	12 MeV^A	2.85	2.85	0.00 %
# Applicator:	16 MeV^A	3.29	3.35	1.82 %
(15×15) cm^2	20 MeV^A	2.39	2.45	2.51 %
	6 MeV^A	1.40	1.45	3.57 %
# Square cutout:	9 MeV^A	2.20	2.05	6.81 %
(20×20) cm^2	12 MeV^A	2.89	3.05	5.53 %
# Applicator:	16 MeV^A	3.10	3.15	1.61 %
(20×20) cm^2	20 MeV^A	2.39	2.35	1.67 %
# Rectangular cutout:	6 MeV^A	1.25	1.25	0.00 %
(3×8) cm^2	9 MeV^A	1.85	1.85	0.00 %
# Applicator:	12 MeV^A	2.15	2.15	0.00 %
(10×10) cm^2	16 MeV^A	2.25	2.15	4.40 %
# Circular cutout:	6 MeV^A	1.25	1.35	8.00 %
Radius = 2.5 cm	9 MeV^A	1.95	2.05	5.13 %
# Applicator :	12 MeV^A	2.65	2.65	0.00 %
(10×10) cm^2	16 MeV^A	2.55	2.35	7.80 %
				
# Irregular cutout:	6 MeV^B	1.01	1.15	13.86 %
At PDD1	9 MeV^B	1.25	1.15	8.00 %
# Applicator:	12 MeV^B	1.46	1.35	7.53 %
(10×10) cm^2	16 MeV^B	1.78	1.35	24.15 %
	20 MeV^B	1.50	1.35	10.00 %
				
# Irregular cutout:	6 MeV^B	1.26	1.25	0.79 %
At PDD2	9 MeV^B	1.60	1.75	9.04 %
# Applicator :	12 MeV^B	1.90	1.95	2.40 %
(10×10) cm^2	16 MeV^B	2.16	2.05	5.24 %
	20 MeV^B	1.87	1.65	12.02 %

TABLE 6–3 – *Tabulated values for the measured and calculated depth of 90% of the maximum dose - R_{90}. Note:* ^{A}*data measured with ionization chamber IC-10 in water phantom. &* ^{B}*data measured with EBT GafChromic® films in Solid Water® phantom.*

Cutout shape & applicator size	Beam Energy E_{nominal} [MeV]	Measured Depth R_{90} [cm]	Calculated Depth R_{90} [cm]	$\left\lvert\frac{R_{90}^{\text{Meas}}-R_{90}^{\text{Cal}}}{R_{90}^{\text{Meas}}}\right\rvert$
	6 MeV^{A}	1.79	1.78	0.69 %
# Square cutout:	6 MeV^{B}	1.78	1.78	0.00 %
(10×10) cm^2	9 MeV^{A}	2.71	2.76	2.09 %
# Applicator:	12 MeV^{A}	3.89	3.94	1.32 %
(10×10) cm^2	16 MeV^{A}	5.12	5.15	0.69 %
	20 MeV^{A}	5.88	6.07	3.23 %
	6 MeV^{A}	1.72	1.78	2.91 %
# Square cutout:	9 MeV^{A}	2.73	2.77	1.45 %
(15×15) cm^2	12 MeV^{A}	3.91	3.94	0.66 %
# Applicator:	16 MeV^{A}	5.07	5.15	1.57 %
(15×15) cm^2	20 MeV^{A}	6.01	6.06	0.93 %
	6 MeV^{A}	1.84	1.81	1.68 %
# Square cutout:	9 MeV^{A}	2.81	2.79	0.49 %
(20×20) cm^2	12 MeV^{A}	3.87	3.96	2.38 %
# Applicator:	16 MeV^{A}	5.06	5.21	2.88 %
(20×20) cm^2	20 MeV^{A}	6.02	6.16	2.29 %
# Rectangular cutout :	6 MeV^{A}	1.70	1.76	3.66 %
(3×8) cm^2	9 MeV^{A}	2.58	2.63	1.86 %
# Applicator:	12 MeV^{A}	3.45	3.47	0.67 %
(10×10) cm^2	16 MeV^{A}	4.07	4.01	1.37 %
# Circular cutout:	6 MeV^{A}	1.72	1.79	3.89 %
Radius = 2.5 cm	9 MeV^{A}	2.70	2.76	2.21 %
# Applicator:	12 MeV^{A}	3.74	3.76	0.39 %
(10×10) cm^2	16 MeV^{A}	4.53	4.46	1.54 %
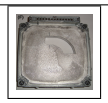				
# Irregular cutout:	6 MeV^{B}	1.64	1.67	1.72 %
At PDD1	9 MeV^{B}	2.16	2.17	0.6 %
# Applicator:	12 MeV^{B}	2.71	2.65	2.53 %
(10×10) cm^2	16 MeV^{B}	3.28	3.06	6.85 %
	20 MeV^{B}	3.30	3.24	1.88 %
				
# Irregular cutout:	6 MeV^{B}	1.75	1.78	1.27 %
At PDD2	9 MeV^{B}	2.54	2.59	2.08 %
# Applicator:	12 MeV^{B}	3.25	3.27	0.41 %
(10×10) cm^2	16 MeV^{B}	3.76	3.81	1.43 %
	20 MeV^{B}	4.10	4.14	1.07 %

TABLE 6–4 – *Tabulated values for the measured and calculated depth of 50% of the maximum dose - R_{50}. Note:* ^{A}*data measured with ionization chamber IC-10 in water phantom &* ^{B}*data measured with EBT GafChromic® films in Solid Water® phantom.*

Cutout shape & applicator size	Beam Energy E_{nominal} [MeV]	Measured Depth R_{50} [cm]	Calculated Depth R_{50} [cm]	$\left\lvert\frac{R_{50}^{\text{Meas}}-R_{50}^{\text{Cal}}}{R_{50}^{\text{Meas}}}\right\rvert$
	6 MeV^{A}	2.38	2.33	2.19 %
# Square cutout:	6 MeV^{B}	2.33	2.33	0.00 %
(10×10) cm^2	9 MeV^{A}	3.51	3.54	0.84 %
# Applicator:	12 MeV^{A}	4.98	4.99	0.17 %
(10×10) cm^2	16 MeV^{A}	6.65	6.67	0.37 %
	20 MeV^{A}	8.33	8.31	0.22 %
	6 MeV^{A}	2.31	2.32	0.49 %
# Square cutout:	9 MeV^{A}	3.54	3.54	0.14 %
(15×15) cm^2	12 MeV^{A}	5.00	4.99	0.07 %
# Applicator:	16 MeV^{A}	6.64	6.66	0.30 %
(15×15) cm^2	20 MeV^{A}	8.32	8.30	0.19 %
	6 MeV^{A}	2.40	2.37	1.09 %
# Square cutout :	9 MeV^{A}	3.59	3.56	0.49 %
(20×20 cm^2	12 MeV^{A}	4.98	5.02	0.68 %
# Applicator:	16 MeV^{A}	6.60	6.64	0.64 %
(20×20) cm^2	20 MeV^{A}	8.38	8.37	0.23 %
# Rectangular cutout:	6 MeV^{A}	2.30	2.32	1.13 %
(3×8) cm^2	9 MeV^{A}	3.48	3.50	0.65 %
# Applicator:	12 MeV^{A}	4.83	4.84	0.29 %
(10×10) cm^2	16 MeV^{A}	6.20	6.18	0.34 %
# Circular cutout:	6 MeV^{A}	2.30	2.33	1.15 %
Radius = 2.5 cm	9 MeV^{A}	3.52	3.55	0.84 %
# Applicator:	12 MeV^{A}	4.98	4.96	0.40 %
(10×10) cm^2	16 MeV^{A}	6.38	6.40	0.31 %
# Irregular cutout : 	6 MeV^{B}	2.37	2.32	2.28 %
At PDD1	9 MeV^{B}	3.35	3.35	0.00 %
# Applicator:	12 MeV^{B}	4.36	4.41	1.21 %
(10×10) cm^2	16 MeV^{B}	5.36	5.43	1.23 %
	20 MeV^{B}	5.98	6.05	1.19 %
# Irregular cutout: 	6 MeV^{B}	2.36	2.35	0.37 %
At PDD2	9 MeV^{B}	3.54	3.52	0.58 %
# Applicator:	12 MeV^{B}	4.82	4.79	0.60 %
(10×10) cm^2	16 MeV^{B}	6.04	6.05	0.22 %
	20 MeV^{B}	7.16	7.13	0.43 %

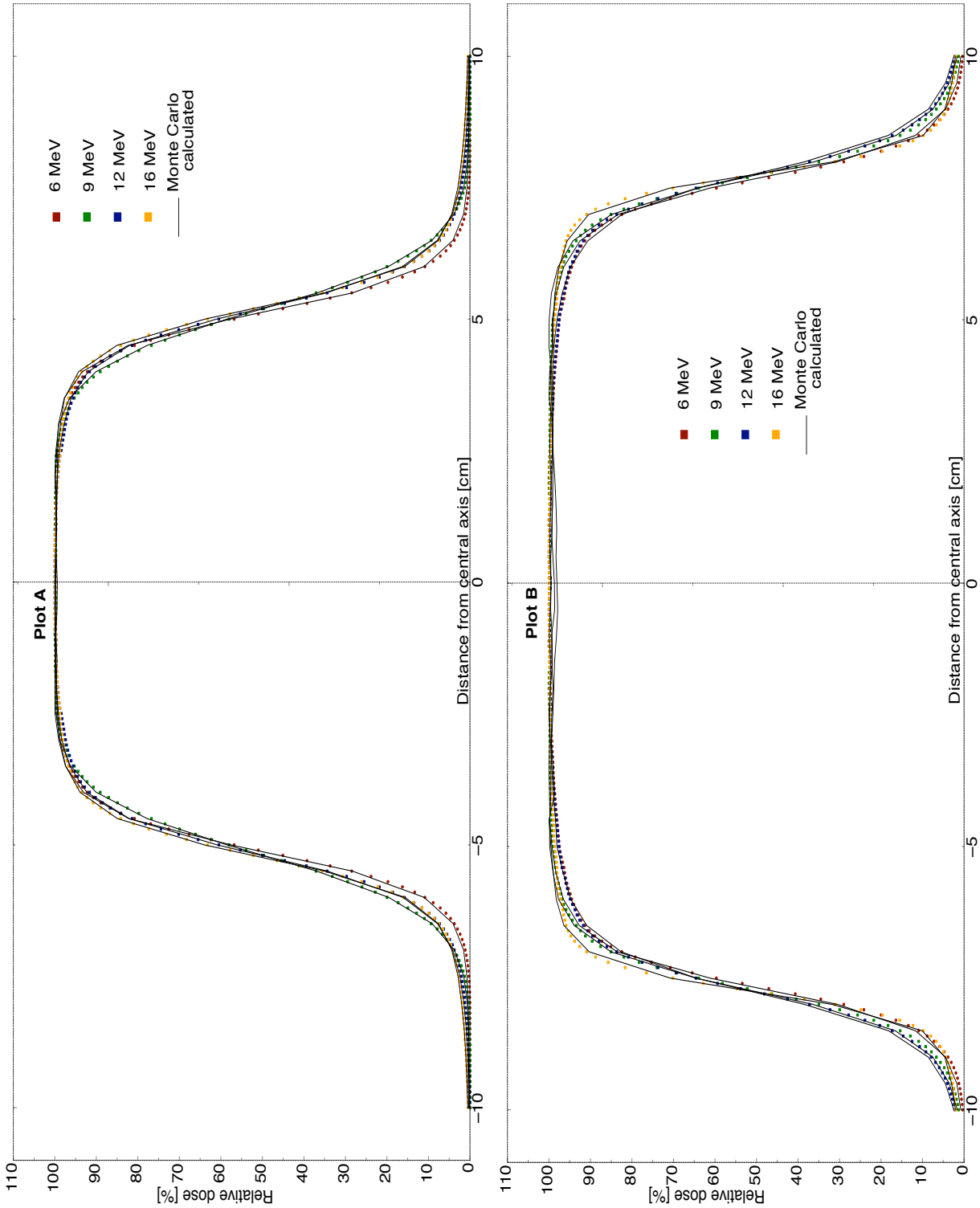

FIGURE 6–6 – *Lateral dose profiles in water at respective Z_{max} for 6, 9, 12 & 16 MeV electron beam at 100 cm SSD calculated with Monte Carlo and measured with ionization chamber IC-10 for*:
Plot A: *(10×10) cm^2 applicator; (10×10) cm^2 square cutout.*
Plot B: *(15×15) cm^2 applicator; (15×15) cm^2 square cutout.*

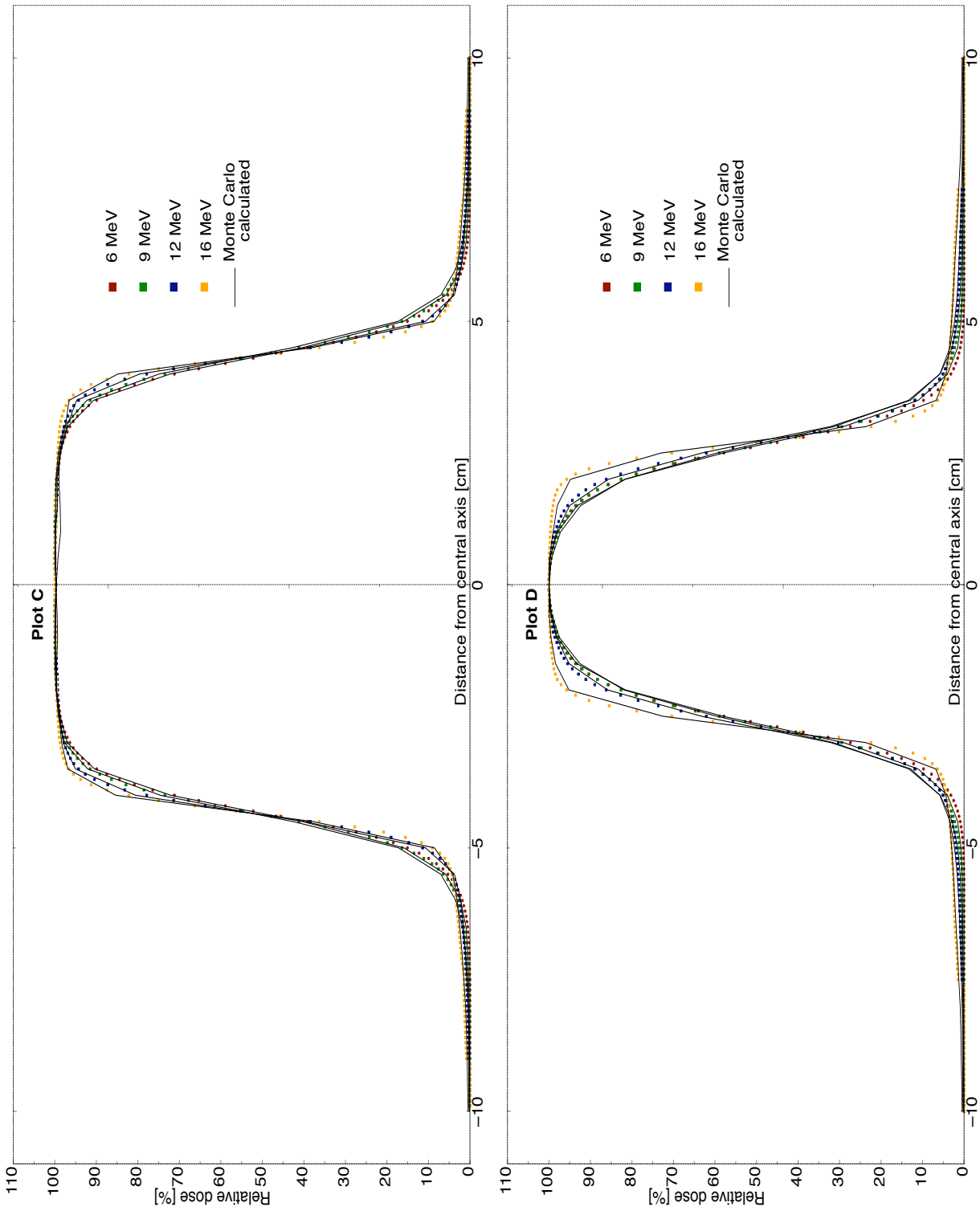

FIGURE 6–7 – *Lateral dose profiles in water at respective Z_{max} for 6, 9, 12 & 16 MeV electron beam at 100 cm SSD calculated with Monte Carlo and measured with ionization chamber IC-10 for*:
Plot C: *(10×10) cm^2 applicator; (3×8) cm^2 rectangular cutout.*
Plot D: *(10×10) cm^2 applicator; circular cutout with 5 cm diameter.*

References

[1] A.W.Wamied, J.P.Seuntjens, F.Verhaegen, F.Deblois, E.B.Podgorsak. Validation of Monte Carlo calculated surface doses for megavoltage photon beams. *Med. Phys.*, 32 :286–98, 2005.

Chapitre 7
CONCLUSION

Contents

7.1 Summary.

The main objective of this project was to build a Monte Carlo model for electron beams of energy 6 to 20 MeV for a Varian Clinac 21-EX. With this model, accurate calculations of dose distributions in water and in Solid Water® phantoms had to be validated for various applicator sizes and field shapes: square, rectangular, circular and irregular. BEAMnrc code was used to simulate the trajectories of particles through the linac treatment head. An isotropic point source with a circular beam of radius 0.04 cm located 5.5 cm above the first component modules was found to give the best agreements. Phase-spaces files were collected at the location of the phantom surface (i.e. 100 cm SSD), and were used as input files for DOSXYZnrc simulations. Set of measured PDDs and profiles has been used to tune-up the model. The results are in very good agreement with measurements, within 2% for R_{50} and R_{90} in most cases. The model was only tested at a source to axis distance of 100 cm but should theoretically work for extended SSD.

These preliminary results have shown that the proposed electron beam model accurately simulates the transport of an electron beam within a water and a Solid Water® phantom. Incorporated into the radiotherapy research environment for Monte Carlo: the McGill Monte Carlo treatment planning - **MMCTP**, the model becomes a very powerful and useful tool to simulate clinical electron beams and obtain dose distributions as well as evaluating commercial treatment planning systems.

Our model incorporated within an in-house TPS could also alleviate the commissioning measurement load. This includes calculations of output factors for clinical electron beams, simulation of depth-dose curves and profiles at depth of clinical interest for small field size cutouts. Furthermore, our proposed model offers a powerful tool to better understand the physics related to electron beam interactions with matter. The overall idea and strategy used in this research should also work for any other type of linear accelerator. Indeed, it is believed that for most clinical accelerators of the same type, their treatment head designs are exactly the same or at least very similar, therefore the proposed electron beam model can, not only be applied for a Varian Clinac 21-EX, but also for any other accelerator of the same type such as the Varian Clinac 23-IX or the Varian Trilogy. For any other type of linear accelerator, the different components should be modeled and adjusted to accurately simulate the dose distribution.

7.2 Future work.

Our electron beam model should be further tested in various situations. For instance, a major task in commissioning an electron accelerator is to measure relative output factors versus cutout size. Due to time constraints, this step was unfortunately not performed, but the next logical step would be to verify the performance of our electron beam model to calculate accurately output factors. Other future work could also include dose calculations in inhomogeneous phantoms, in order to study the accuracy of our model to calculate dose deposition within different media. For instance, measuring and calculating the dose within a phantom composed of water, lung, and bone would be an important experiment de conduct.

Most of the measured data was collected with an IC-10 cylindrical ion chamber. However, due to the relatively large size of the chamber relative to the very small

cutout size used for this work, GafChromic® EBT films were chosen as a better alternative. Diodes and TLD (Thermo Luminescent Dosimeter) would allow verifications of our measurements against the data obtained with ionization chamber. An other example would have been the use of a phantom embedded extrapolation chamber (PEEC) made of Solid Water® to validate our calculated doses in the dose build-up region.

All measurements and calculations made in this thesis were performed for vertical beams with a source to axis distance of 100 cm. Investigation of our model to calculate dose for oblique beams and/or extended SSD would be necessary.

A set of in-air energy distribution measurements would also provide interesting information about the beam behavior before hitting the water phantom. This would allow us to obtain a more insightful understanding and accurate description of the source geometry.

Other future work could include the verification of our model to calculate more realistic clinical plans. This would include for example verification of dose calculations in CT patients against dose calculated with Eclipse and Cadplan TPS.

There are numerous research projects under development that require accurate dose calculation for electron beams. For example, a very promising technique is the energy modulated electron therapy (EMET) that uses a novel few-leaf electron collimator (FLEC). Our model would certainly help during the commissioning of this new technique.

ABBREVIATIONS

AAPM	American Association of Physicists in Medicine
CPU	Central processing unit
CM	Component module
CSDA	Continuously slowing down approximation
EGS	Electron-Gamma-Shower
EBF	Electron Backscatter Factor
ETRAN	Electron Transport
ESTRO	European Society for Therapeutic Radiology and Oncology
FS	Field size
FWHM	Full width at Half Maximum
FLUKA	fluktuierende kaskade
GEANT	GEometry ANd Tracking
GUI	Graphical User Interface
IAEA	International Atomic Energy Agency
ICRP	International Commission on Radiological Protection
ICRU	International Commission on Radiation Units and Measurements
JGH	Jewish General Hospital
Linac	Linear Accelerator
MC	Monte Carlo
MV	Megavoltage
MU	Monitor Unit
MGH	Montreal General Hospital
NACP	Nordic Association of Clinical Physicists

NIST	National Institute of Standards and Technology
PDD	Percent depth dose
PDI	Percent depth Ionization
PSF	Phase space file
PTV	Planning target volume
PENELOPPE	Penetration and Energy Loss of Positron and Electron
SSD	Source-to-surface distance
SAD	Source-to-axis distance
TIFF	Tagged Image File Format
TG	Task Group
TPS	Treatment Planning System

REFERENCES

[1] K. R. Hogstrom, M. D. Mills, and P. R. Almond. Electron beam dose calculations. *Phys. Med. Biol*, 26 :445–459, 1940.

[2] E. Mah J. Antolak J. W. Scrimger and J. J. Battista. Experimental evaluation of a 2D and 3D electron pencil beam algorithm. *Phys. Med. Biol.*, 34 :1179–1194, 1989.

[3] J. Cygler J. J. Battista J. W Scrimger E. Mah and J. Antolak. Electron dose distributions in experimental phantoms ; a comparison with 2D pencil beam code. *Phs. Med. Biol.*, 32 :1073–1086, 1987.

[4] K. R. Shortt, C. K. Ross, A. F. Bielajew, and D. W. O Rogers. Electron beam dose distributions near standard inhomogeneities. *Phs. Med. Biol.*, 31 :235–249, 1986.

[5] Mackie T R. Application of the Monte Carlo method in radiation therapy. *The dosimetry of Ionization Radiation*, 3 :541 – 620, 1990.

[6] Mohan R and Antolak. Monte Carlo techniques should replace analytical methods for estimating dose distribution in radiotherapy treatment planning. *Med Phys*, 28 :123–126, 2001.

[7] Rogers D W and Bielajew A F. Monte Carlo techniques of electron and photon transport for radiation dosimetry. *The dosimetry of Ionization Radiation*, 3 :427–539, 1990.

[8] Rogers D W and Bielajew A F. The role of Monte Carlo simulation of electron transport in radiation dosimetry. *Int. J. Radiat. Appl. Instrum*, 42 :965–74, 1991.

[9] York E Wang L and Chui C S. Monte Carlo evaluation of 6 MV intensity modulated radiotherapy plans for head and neck and lung treatments. *Med. Phys.*, 29 :2705–2717, 2002.

[10] Pawlicki T and Ma C M. Monte Carlo simulation for MLC-based intensity-modulated radiotherapy. *Med. Dosim.*, 26 :157–168, 2001.

[11] Epp E.R. Johns H.E., Bates L.M. 1,000-curie cobalt 60 units for radiation therapy. *Nature*, 168 :1035–6, 1951.

[12] Varian Medical System Web-Page. http ://www.varian.com/.

[13] Ervin.B. Podgorsak. *Radiation Physics for Medical Physicists*, volume 1 edition. Springer Berlin Heidelberg New York., New York, 2005.

[14] Rogers D W O, Faddegon B A, Ding G X, Ma C M, Wei J, and Mackie T R. BEAM : A Monte Carlo code to simulate radiotherapy treatment units. *Med. Phys.*, 22 :503–524, 1995.

[15] Rogers DWO, Ma Ding, GX Walter, Sheikh-Bagheri and Zhang GC. BEAMnrc users manaual. Pirs 509a (rev f), NRCC - Canada Ottawa - National Research Council., 2001.

[16] Walters B, Kawrakow I, and Rogers D W O. DOSXYZnrc users manual. PIRS 794revB, NRCC, 2004.

[17] Kawrakov I and Rogers D W O. The EGSnrc code system : Monte Carlo simulation of electron and photon transport. Pirs-701, NRCC - Canada Ottawa - National Research Council., 2003.

[18] Kawrakov I and Rogers D W O. EGSnrc / BEAMnrc / DOSXYZnrc. EGS electron gamma source. Pirs, NRCC - Canada Ottawa - National Research Council., 2003.

[19] C.Möller. Zur theories des durchgangs schneller elektronen durch materie. *Ann. Phys.*, 14 :468–577, 1932.

[20] ICRU. Stopping powers for electrons and positrons. PIRS 37, ICRU - International Commission on Radiation Units and Measurements, Washington, D.C, 1984.

[21] ICRU. Radiation dosimetry : Electron beams with energies between 1 and 50 MeV. PIRS 35, ICRU - International Commission on Radiation Units and Measurements, 1984. Bethesda, Maryland.

[22] ICRU. Radiation dosimetry : Electrons with initial energies between 1 and 50 MeV. PIRS 21, ICRU - International Commission on Radiation Units and Measurements, 1972. Bethesda, Maryland.

[23] NACP. Procedures in external radiation therapy dosimetry with electron and photon beams with maximum energies between 1 and 50 MeV. Acta Radiol. 19 :55, Nordic Association of Clinical Physics (NACP)., 1980.

[24] Briesmeister J F. A protocol for the determination of absorbed dose from high energy photon and electron beams. Technical Report Task group Number 21, AAPM - American Association of Physicists in Medicine., 1983.

[25] Harder D. Energiespectren scgneller elecktronen in verschiedenen tiefen. in : Monstreux, zuppinger a, poretti g, eds. symposium on high-energy electrons. *Springer-Verlag - Berlin*, 26 :260, 1965.

[26] G. X. DING D.T. BURNS and W. O. Rogers. R_{50} as a beam quality specifier for selecting stopping-power ratios and reference depths for electron dosimetry. *Med. Phys.*, 23 :383–388, 1996.

[27] Constantinou C Attix FH Paliwal BR. A SolidWater® phantom material for radiotherapy x-ray and gamma-ray beam calibrations. *Phs. Med. Biol.*, 9 :436–41, 1982.

[28] CERN. GEANT - GEometry ANd TRacking. Technical report, CERN - European Organization for Nuclear Research., 1982.

[29] INFN CERN. FLUKA - (FLUktuierende KAskade). Technical report, Italian National Institute for Nuclear Physics (INFN) and by the European Organization for Nuclear Research (CERN)., 1982.

[30] UB. PENELOPPE - PENetration and energy LOss of Positron and Electron. Technical report, Universitad de Barcelona, 1982.

[31] Briesmeister J F. MCNP - a general Monte Carlo N-particle transport code version 4C. Technical Report LA-12625-M, Los Alamos Natl. Lab., 2000.

[32] Berger and Seltzer. ETRAN - electron transport. Technical report, National Institute of Standars and Technology, 1968.

[33] Nordic Association of Clinical Physics NACP Andreo et al. MCEF source code - Monte Carlo for Evaporation-Fission calculations. Technical report, University of Zaragoza, Spain Karolinska Institute-University of Stockholm, Sweden, Andres, 1988.

[34] M.J Berger. Monte Carlo calculation of the penetration and diffusion of fast charged particles. *Nucl. Instrum. Methods Phys. Res.*, 134 :135–215, 1963.

[35] Kawrakow I. Accurate condensed history Monte Carlo simulation of electron transport II. application to ion chamber response simulation. *Med. Phys.*, 27 :499–513, 2000.

[36] Rogers D W O Nelson W R and Hirayama H. The EGS4 code system. *Stanford Linear Accelerator Center Report - SLAC*, 1 :265, 1985.

[37] Kawrakov I and Rogers D W O. The EGSnrc system status report from advanced Monte Carlo for radiation physics, particle transport simulation and applications. In *proceedings of the Monte Carlo 2000 Conference*, Lisbon, October 2000. NRCC - Canada Ottawa - National Research Council., Springer.

[38] W.R. Nelson. PEGS4 : datasets for different media - Course on Electron and Photon Transport using the EGS4 Monte Carlo System. In UK National Physical Laboratory, Teddington, editor, *EGS4 : datasets for different media*, volume Lecture 9. Stanford Linear Accelerator Center, September 1989.

[39] IAEA. Absorbed dose determination in external beam radiotherapy - an international code of practice for dosimetry based on standards of absorbed dose to water. Technical Report Technical report Series No. 398, IAEA - International Atomic Energy Agency., 2000. Sponsored by the IAEA, WHO, PAHO and ESTRO.

[40] Slobodan Devic, Jan Seuntjens, Gyorgy Hegyi, and Ervin B. Podgorsak. Dosimetric properties of improved gafchromic™ films for seven different digitizers. *Med. Phys.*, 31, September 2004.

[41] Slobodan Devic, Jan Seuntjens, Edwin Sham, and Ervin B. Podgorsak. Precise radiochromic™ film dosimetry using a flat-bed document scanner. *Med. Phys.*, 32, July 2005.

[42] Slobodan Devic, Nada Tomic, Zhiyu Pang, Jan Seuntjens, and Ervin B. Podgorsak. Absorption spectroscopy of EBT model GAFCHROMIC™ film. *Med. Phys.*, 34, January 2007.

[43] Slobodan Devic, Nada Tomic, Christopher G. Soared, and Ervin B. Podgorsak. Optimizing the dynamic range extension of a radiochromic™ film dosimetry system. *Med. Phys.*, 36, February 2009.

[44] Montreal General Hospital. Varian oncology systems, Monte Carlo project. Information Serial Number 60A, Varian, 2004.

[45] Claude Albaret. Automated system for Monte Carlo determination of cutout factors of arbitrary shaped electron beams and experimental verification of Monte Carlo calculated dose distribution. Master's thesis, McGill University, Montreal General Hospital 1650 avenue cedar Montreal, Quebec H3G 1A4, 2004.

[46] Jurgen Last. Cutout Manager - A stand-alone software system to calculate output factors for arbitrarily shaped inserts with Monte Carlo technique. Master's thesis, McGill University, Montreal General Hospital 1650 avenue cedar Montreal, Quebec H3G 1A4, 2008.

[47] Genevieve Jarry. *Study of Novel Techniques for Verification Imaging and Patient Dose Reconstruction in External Beam Radiation Therapy*. PhD thesis, McGill University, Montreal General Hospital - 1650 avenue Cedar Montreal Quebec H3G 1A4, 2007.

[48] Alexander A, DeBlois F, and Seuntjens J. MMCTP a radiotherapy research environment for Monte Carlo and patient-specific treatment planning. *Med. Phys.*, 33 :2293, 2006.

INDEX